Stony Brook University

Interactive Software Systems for Planar Parallel Manipulator- and Spherical Four-Bar Linkage- Design

A Thesis Presented

by

Kartik Thakkar

to

The Graduate School

in partial fulfillment of the

Requirements

for the degree of

Master of Science

in

Mechanical Engineering

Stony Brook University

December 2012

Stony Brook University
The Graduate School

Kartik Thakkar

We, the thesis committee for the above candidate for the
Master of Science degree, hereby recommend
acceptance of this thesis.

Dr. Anurag Purwar, Advisor,
Research Associate Professor, Mechanical Engineering Department

Dr. Q. Jeffrey Ge, Chairman of Thesis Committee
Professor, Mechanical Engineering Department

Dr. Yu Zhou,
Assistant Professor, Mechanical Engineering Department

This thesis is accepted by the Graduate School.

Charles Taber
Interim Dean of the Graduate School

Abstract of the Thesis

Interactive Software Systems for Planar Parallel Manipulator- and Spherical Four-Bar Linkage- Design

by

Kartik Thakkar

Master of Science

in

Mechanical Engineering

Stony Brook University

2012

Dimensional Synthesis is of crucial importance in robotics for trajectory planning, task specification in Mechanism Synthesis,CNC tool path planning as well as in micro and nano systems, where kinematics plays an important role. This thesis presents an interactive software for the dimensional synthesis of planar parallel manipulators (PPMs) and spherical four bar motion approximation from a given set of displacements.

For PPMs, a user friendly and interactive graphical software has been developed for the synthesis using C++,OpenGL and Qt. The software is designed and implemented using an Object Oriented Programming (OOP) architecture. This architecture naturally maps mathematical formulation of the constraints of PPMs to the OOP paradigm and enables extending the software to handle other types of linkages as well. Using the kinematic mapping approach, the mechanism design problem is transformed into a problem of manipulation of surfaces to visually contain the image curve by simple geometric manipulation of the size, orientation,and location of the constraint surfaces which are developed for all the cases and that yields the desired mechanism.

For Spherical Four Bar, a web based software using *Mathematica* has been

developed. The software finds a spherical 4-bar mechanism that best guides through the set of given displacements. It implements an efficient linear algorithm that naturally extracts the geometric constraints of a motion and leads directly to a mechanism for motion generation.

The entire process for both the softwares is intuitive and lends designers an understanding of the mechanism design methodology.

Contents

List of Figures

List of Tables

ACKNOWLEDGEMENT

Although I have no “loving wife” to thank for keeping the children away while I wrote this thesis, I do have many friends and professors who have contributed to this success. I take this opportunity to thank my research advisor, Prof. Anurag Purwar,for his invaluable support, guidance and for instilling in me, the spirit of research. He has been the best mentor that anyone can hope for.

I would also like to extend my thanks to Prof. Jeff Ge for agreeing to chair and Prof. Yu Zhou for being a member of my thesis committee.My lab mates,Xiangyun Li and Ping Zhao, for their timely assistance, support and immense patience in answering my seemingly unending list of questions.

My parents have been my backbone and have stood by me throughout. I am deeply indebted to them, none of this would have been possible without their encouragement and faith in my capabilities. Last but not the least,there are two people who deserve special appreciation, Milind Ranade and Niveda Naik, I cannot thank them enough.

In the past one and half year, as a graduate student of Stony Brook University, I have learned at lot and grown as a person. The environment here has been educating, inspiring and pleasant. I am now confident and well rounded in all specialties and have a vision of how I see myself grow in the future. I owe a lot to Prof. Anurag Purwar, my advisor and mentor.

Chapter 1

Introduction and Background

1.1 Introduction

In motion generation, a few positions or the motion of the coupler is given and we have to find the mechanism that best approximates the given positions. This thesis deals with the problem of dimensional synthesis of planar parallel manipulators and spherical four bar linkages for motion generation. In this chapter a general overview of the existing work in the area of dimensional synthesis of planar parallel manipulator and synthesis of spherical four bar is discussed.

A planar parallel manipulator is treated as an assembly of three open chains connected to a moving platform. Each open chain imposes kinematic constraints that limit the positions and orientations of the object connected to the end link. We use the algebraic form of the constraint manifold for the

planar open chains. Thus, the kinematic constraints are transformed into geometric constraints, and the given rational motion is transformed into a rational curve in the image space. This way, the problem reduces to finding the constraint manifold that accommodates the given rational curve. These constraint manifolds can be manipulated so as to change their location, orientation, and the mean curvature. Algebraically, the kinematic constraints are derived in the inequality form, where the limits of the inequalities are functions of link lengths, while the constraint functions themselves incorporate parameters that describe the location and orientation of fixed and moving frames. In the end, we design open chains that simultaneously satisfy the kinematic constraints and the motion requirements. A visual interpretation of this approach is that, we find the smallest possible pair of constraint manifolds that will contain the given image curve entirely in the volume between them.

For Planar Parallel Manipulator, the work presented can be used for synthesis of mechanisms and for trajectory verification. For trajectory verification, the designer can just input the mechanism parameters available and the desired motion of the moving platform, and upon inputting of these parameters, if the interpolated image curve is fully contained in the volume between the pair of constraint manifolds for each leg configuration, it can be validated that the mechanism will be able to perform the desired task.

For spherical bar mechanism, the work presented is an extension of Ge et al. [1] in planar case to spherical four-bar linkage and the approach simply consist of two steps. Since the formulated data fitting process is in linear form,

the first step is finding a pencil of general quadratic manifolds in the image space that best fit the given image points in the least squares sense, which is done by using Singular Value Decomposition and solving for the singular vectors. The singular vectors associated with the smallest singular values are then linearly combined to define the coefficients of a pencil of quadrics. Secondly, four additional constraints on the linear coefficients are then imposed to identify the quadric that qualified to represent a spherical circular constraint from the pencil of quadrics. After the inverse computation converting the quadric coefficients to the spherical four bar parameters, a spherical four bar linkage that best guides through the set of given displacements can be obtained.

1.2 Background

Kinematic synthesis is one of the most common problems in the study of mechanisms and linkages (see Sandor and Erdman [52], Suh and Radcliffe [53], and McCarthy [54]), and there has been a great deal of academic research in the development of software systems for the synthesis of mechanisms (KINSYN III from Rubel and Kaufamn [39], LINCAGES from Erdman and colleagues [40, 41], Kihonge et al. [42], Spades from Larochelle [43], Perez and McCarthy [47], Su and McCarthy [48], Synthetica from Su et al. [49]). In the commercial domain, SyMech [50] and WATT [51] are two well-known software systems for planar mechanisms design.

In the past several years, significant amount of research has been done in

the application of well-known curve and surface design algorithms for the purpose of developing rational Bezier and B-Spline motions of rigid bodies. The idea behind such a synergy is that the problem of designing rational curves in a higher dimensional projective space via a special mapping. By choosing the quaternion representation of the displacement and orientation, the problem is further reduced to designing curves in the space of quaternions. Rational motions, with applications spanning across areas such as motion animation in computer graphics, task specification in mechanism synthesis, and virtual reality systems as well as Cartesian motion planning in robotics, are an attractive proposition since they integrate well the industry standard nonuniform rational B-spline(NURBS) based computer aided design/computer aided manufacturing(CAD/CAM) system. Furthermore, from a computational perspective they can easily exploit fast and stable algorithms from CAGD.

The concept of kinematic mapping approach for dimensional synthesis of planar and spherical mechanisms was pioneered by Ravani and Roth [10].In the kinematic mapping approach to kinematic synthesis, both planar and spherical displacements in Cartesian Space can be mapped into points in a three-dimensional projective space (called Image Space of Planar or Spherical Kinematics), while workspace constraints of a mechanism map into algebraic manifolds in the same space Their work was followed by Bodduluri and McCarthy [25], Bodduluri [27], and Larochelle [28]. Their approach involved minimizing the distance error between the given positions and the image curve of the chain. This resulted in an approximate motion synthesis. Venkataramanu-

jam and Larochelle [31] used parametrized constraint manifolds and employed non-linear optimization to give numerical methods for approximate motion synthesis of open and closed chains.

To study the dimensional synthesis problem from the perspective of constrained motion interpolation, Jin and Ge [65] and Purwar and Jin [66] have studied the problem of motion interpolation under kinematic constraints for planar and spherical 6R closed chains. By using quaternions or dual quaternions and kinematic mapping approach, the problem of constrained motion interpolation was transformed into a problem of designing a rational curve constrained to satisfy geometry of the constraint manifold. Starting with an initial unconstrained curve, the curve was manipulated using an iterative numerical method until it fits inside the constraint manifold. The current work investigates the inverse problem, that is, to manipulate the constraint manifold while keeping the given rational curve fixed for dimensional synthesis. Jun et al. [37] initially designed and developed a system for the dimensional synthesis of planar 6R mechanisms, this system was then further developed to account for planar parallel manipulators by Purwar and Gupta [67]. This system was limited to the use of RRR and RPR configurations only.The extension of this work covered by Purwar and Anantwar [19] included five other configurations namely RRP, RPP, PRP, PRR and PPR.

Compared to dimensional synthesis, type synthesis is a much less researched subject. Nonetheless, there exists a sizable amount of literature, especially for the case of planar mechanisms. The main approaches include augmentation of

polygonal-link patterns through introduction of binary links; transformation of binary chains; building up of desired chains by addition of links to simpler chains with fewer links; and direct algebraic determination of matrices representing chains. The tools used to implement these approaches can be based on direct visual inspection and intuition, graph theory, group theory or matrix representation based algebraic procedures. The focus of all these work, however, is not on the task to be accomplished but rather on the classification and enumeration of mechanisms. A comprehensive review of research in this area can be found in [91]. In spite of all the advances in this area, type synthesis remains to be the most elusive part of the mechanism design process.

Spherical mechanisms constrain the motion of a moving object on the surface of a sphere and all the moving surfaces are concentric spheres. They are compact and provide a wide range of transmission characteristics (Chiang [17]).

For computer aided design of spherical mechanisms, McCarthy, Larochelle, Vance, and colleagues have devoted their efforts to the design of spherical four bar mechanisms in traditional Human Computer Interaction (HCI) as well as virtual reality (VR) environment for the motion guidance through a given number of positions (see Sphinx from Larochelle et al. [44], Sphinxpc from Ruth and McCarthy [45], SphinxVR from Furlong et al. [20], Osiris from Tse and Larochelle [46]). Ketchel and Larochelle [21] also developed SphinxCAM to aid in automated assembly and manufacturing of spherical 4R mechanisms designed in systems such as Sphinx and Osiris. Kraal and Vance et al. [18] recognized the need to develop user interfaces that were better suited to the

cognitive and perceptive nature of designers. Their efforts led to VEMCES, a virtual reality interface for spherical four bar mechanism design.

However most of the solutions to the design of mechanisms for approximated motion synthesis requires a complicated algorithm and in general they are inefficient.Ge et al. [1] proposed a simple and fast algebraic method for planar fourbar linkages synthesis, which uncovers the geometric constraint hidden in the given motion via a linear, two step method.A single degree of freedom motion of a planar or spherical mechanism is represented by the intersection curve of two algebraic manifolds.The problem of motion approximation is transformed into a algebraic curve fitting problem in the image space, where various methods in approximation theory may be applied. This includes the definition of the approximation error(called structural error) in the image space, formulation of a least squares problem and application of appropriate numerical methods to find values of the design variables for minimization of the error. Hayes et al. [29, 3]have presented preliminary results for combining type and dimensional synthesis of planar mechanisms for multi-pose rigid body guidance. Existing work on this topic includes [2, 4, 27, 7, 34, 26], in which Ruth and McCarthy [26] described the implementation of spherical four orientation synthesis in the software `SphinxPC`, which encodes a new formulation of classical Burmester theory based on the equation of a spherical triangle which yields a convenient parameterized equation for the central-axis cone. Purwar et al. [2] brings together the kinematics of spherical robot arms and freeform rational motions to study the problem of synthesizing constrained rational

motions for Cartesian motion planning, and realized the synthesis of spherical 2R and 3R robot arms. Also based on kinematic mapping, Husty et al.[34] proposed an approach to the five spherical position synthesis by converting the design problem into a polynomial of degree six. Most of these works either focus on a finite spherical position synthesis or involves a great amount of computation.

The rest of the thesis is organized as follows. Chapter 2 deals with kinematic constraint equations and manifolds of planar parallel manipulator. Chapter 3 discusses about the software architecture and working. Chapter 4 is a guide to use the software tool developed for dimensional synthesis. Chapter 5 discusses about the synthesis of spherical four bar linkages using algebraic fitting method.

Chapter 2

Constraint Manifold for Planar Parallel Manipulator

2.1 Introduction

The kinematic constraints specify the positions and orientations obtainable by a certain link of the chain. In this chapter we discuss the constraint manifold associated with the kinematic constraints of planar parallel manipulator. (See McCarthy [12] and Ge [68])

The organization of the chapter is as follows. Section 2.2 explains the classification of different open chains used as the legs for planar parallel manipulators, section 2.3 explains planar displacements and planar quaternions, and section 2.4 explains the derivation and kinematic constraint equation and manifolds for the different types of planar open chains.

2.2 Classification of Open Chains for a Three-Legged Planar Parallel Manipulators

A three legged parallel manipulator is a 3 DOF closed loop kinematic chain whose end effectors are linked to a base platform by three independent 3 DOF open loop kinematic chains. Each open loop chain has one active joint and two passive joints. Each chain consists of two types of joints Revolute(R) and Prismatic(P) [35].

The possible combinations of Revolute(R) and Prismatic(P) joints in an 3-legged open loop chain are:

RRR, RPR, RRP, PRR, PRP, PPR, RPP

The PPP chain is not useful and must be excluded as it gives rise to only translation with no change in orientation. Thus, there are seven possible useful open loop kinematic chains.

For a 3 DOF open chain mechanism, there exists one active joint (actuated) and two passive joints. This active joint is represented with an underscore. There are 21 3-DOF legs in total (Table 2.2) [70]. The three configurations represented with a cross mark (marked with ^{X}) do not yield 3-DOF planar parallel manipulators (they contain only one controllable DOF). Also, there are eight pairs of symmetric legs, where each pair leads to two kinematically

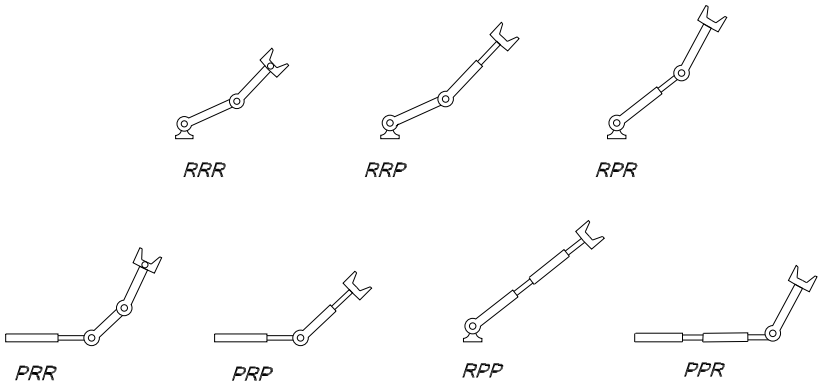

Figure 2.1: All possible useful 3 DOF mechanisms

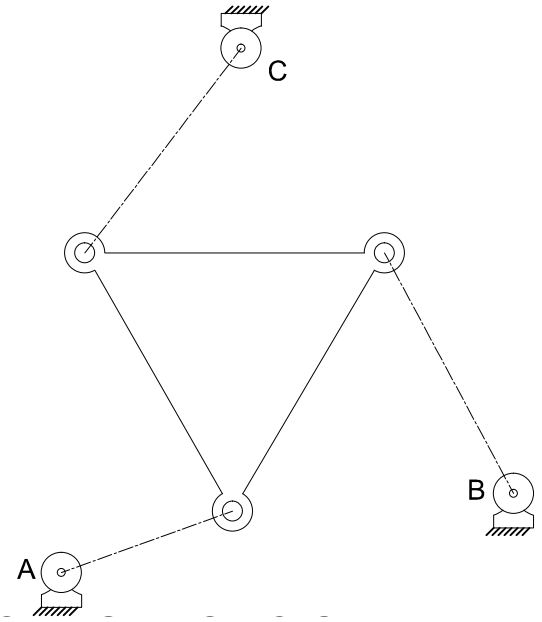

Figure 2.2: A Planar Parallel Manipulator

equivalent planar parallel manipulators. Therefore, these eight legs are eliminated (marked with ˜), which leaves us with only ten configurations.

Table 2.1: All possible 3-DOF planar legs

$\underline{\mathrm{R}}\mathrm{RR}$	$\underline{\mathrm{R}}\mathrm{PR}$	$\underline{\mathrm{R}}\mathrm{PP}^X$	$\underline{\mathrm{P}}\mathrm{RR}$	$\underline{\mathrm{P}}\mathrm{RP}$	$\underline{\mathrm{P}}\mathrm{PR}$	$\underline{\mathrm{R}}\mathrm{RP}$
$\mathrm{R}\underline{\mathrm{R}}\mathrm{R}$	$\mathrm{R}\underline{\mathrm{P}}\mathrm{R}$	$\mathrm{R}\underline{\mathrm{P}}\mathrm{P}$	$\mathrm{P}\underline{\mathrm{R}}\mathrm{R}$	$\mathrm{P}\underline{\mathrm{R}}\mathrm{P}^X$	$\mathrm{P}\underline{\mathrm{P}}\mathrm{R}^{\sim}$	$\mathrm{R}\underline{\mathrm{R}}\mathrm{P}^{\sim}$
$\mathrm{RR}\underline{\mathrm{R}}^{\sim}$	$\mathrm{RP}\underline{\mathrm{R}}^{\sim}$	$\mathrm{RP}\underline{\mathrm{P}}^{\sim}$	$\mathrm{PR}\underline{\mathrm{R}}^{\sim}$	$\mathrm{PR}\underline{\mathrm{P}}^{\sim}$	$\mathrm{PP}\underline{\mathrm{R}}^X$	$\mathrm{RR}\underline{\mathrm{P}}^{\sim}$

2.3 Planar Displacements and Planar Quaternions

A planar displacement can be represented by a planar quaternion (see Bottema and Roth [11] and McCarthy [12]). Planar quaternions have been used for designing planar open chains (Ravani and Roth [9], Larochelle [72], Murray et al. [36], Perez and McCarthy [71]).

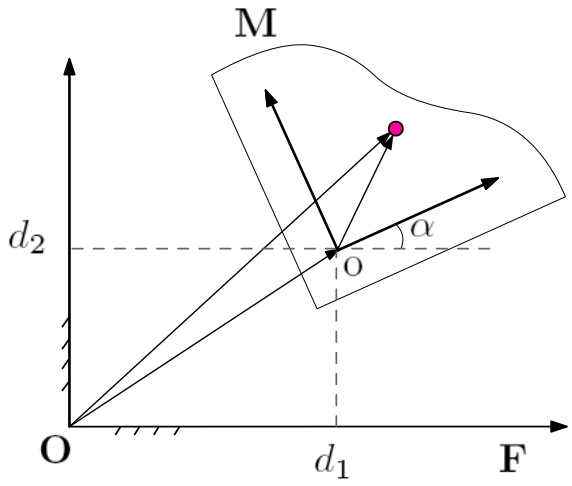

Figure 2.3: A planar displacement.

For a planar displacement shown in Fig. (2.3), let d_1, d_2 denote the coordinates of the origin of the moving frame **M** in the fixed frame **F** and α

denote the rotation angle of $\mathbf{M}$ relative to $\mathbf{F}$. Then a planar displacement can be represented by a planar quaternion, $\mathbf{Z} = Z_1\epsilon\mathbf{i} + Z_2\epsilon\mathbf{j} + Z_3\epsilon\mathbf{k} + Z_4$, where ($\mathbf{i}$, $\mathbf{j}$, $\mathbf{k}$, 1) form the quaternion basis and ϵ is the dual unit with the property $\epsilon^2 = 0$. The components of the planar quaternion, $\mathbf{Z} = (Z_1,\ Z_2,\ Z_3,\ Z_4)$, are given by

$$\begin{aligned} Z_1 &= (d_1/2)\cos(\alpha/2) + (d_2/2)\sin(\alpha/2), \\ Z_2 &= -(d_1/2)\sin(\alpha/2) + (d_2/2)\cos(\alpha/2), \\ Z_3 &= \sin(\alpha/2), \\ Z_4 &= \cos(\alpha/2). \end{aligned} \tag{2.1}$$

These four components can be identified as co-ordinates of a point in four dimensional space. The point $\mathbf{Z}$ is called the *image point of a planar displacement*. The set of image points that represent all planar displacements is called the *image space* of planar displacements and is denoted as Σ_p. In view of Eq.(2.1), the coordinates of an image point must satisfy the equation:

$$Z_3^2 + Z_4^2 = 1. \tag{2.2}$$

The above equation may be interpreted as defining a hyper-circular cylinder in four dimensions.

$$\mathbf{X} = \mathbf{Z}\mathbf{x}\mathbf{Z}^*, \tag{2.3}$$

where $\mathbf{Z} = Z_4 - Z_1\epsilon\mathbf{i} - Z_2\epsilon\mathbf{j} - Z_3\mathbf{k}$ is the *conjugate* of $\mathbf{Z}$.

We can use homogeneous transform matrix to represent Eq.(2.3)

$$\begin{bmatrix} \mathbf{X} \\ 1 \end{bmatrix} = [A] \begin{bmatrix} \mathbf{x} \\ 1 \end{bmatrix}, \tag{2.4}$$

where

$$[A] = \frac{1}{Z_3^2 + Z_4^2} \begin{bmatrix} Z_4^2 - Z_3^2 & -2Z_3Z_4 & 2(Z_1Z_4 - Z_2Z_3) \\ 2Z_3Z_4 & Z_4^2 - Z_3^2 & 2(Z_1Z_3 + Z_2Z_4) \\ 0 & 0 & Z_3^2 + Z_4^2 \end{bmatrix}. \tag{2.5}$$

Note that when Z_i $(i = 1, 2, 3, 4)$ is replaced by wZ_i, where w is a non-zero scalar, the matrix $[A]$ is unchanged. From this perspective, the four components of a planar quaternion can also be considered as a set of homogeneous coordinates for a planar displacement.

Quaternion algebra is also used for composing two successive planar displacements. Let $\mathbf{Z}_0, \mathbf{Z}_1$ denote two planar displacements. The composition of two planar displacements $\mathbf{Z}_1$ followed by $\mathbf{Z}_0$ is given by the quaternion product $\mathbf{Z}_0\mathbf{Z}_1$.

2.4 Kinematic Constraint Equations and Manifolds of Planar Open Chains

In this section, the kinematic constraint equations for all the seven planar open chain configurations (RRR, RPR, RRP, PPR, PRR, PRP, RPP) have

been derived, and their standard form along with the constraint manifolds representing these kinematic constraint equations have been shown.

Originally these equations were derived by Aditya and Sagar (see Jin[69], and Purwar, Gupta[67] and [19]), but the formulation was not unified.Here we have re-derived the equations using *Mathematica* to have a unified formulation for all the configurations.

2.4.1 Planar RRR Open Chain

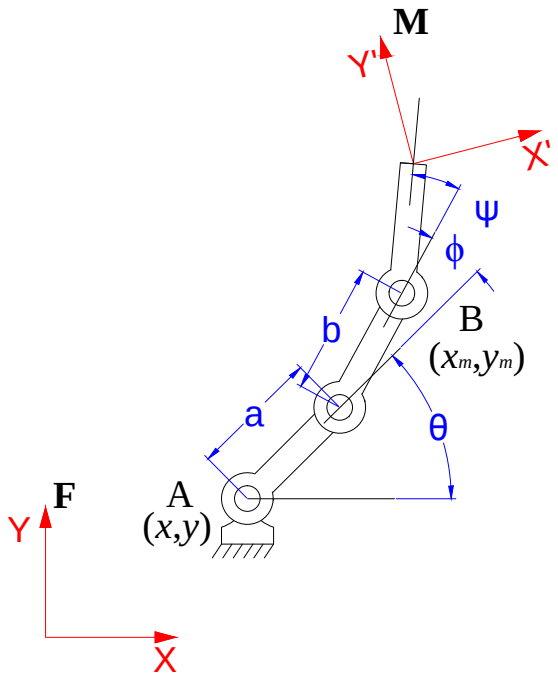

Figure 2.4: A planar RRR open chain

Consider a planar RRR open chain as shown in Fig. 2.4. The length of the first link is a, the length of the second link is b and θ, ϕ, ψ are joint angles for

three revolute joints respectively. In the figure, **F** and **M** mark the fixed and the moving frames, respectively. The fixed pivot is located at (x, y), while the moving frame is located at (x_m, y_m). When the fixed and moving frames are located at A and B respectively the parametrized equation of the constraint manifold $\mathbf{Z}(\theta, \phi, \psi)$ of a RRR robot open chain is obtained as follows:

$$\mathbf{Z}(\theta, \phi, \psi) = \mathbf{Z}(\theta)\mathbf{X}(a)\mathbf{Z}(\phi)\mathbf{X}(b)\mathbf{Z}(\psi). \tag{2.6}$$

The coordinates of $\mathbf{Z}(\theta, \phi, \psi) = (Z_1, Z_2, Z_3, Z_4)$ can be obtained as:

$$\begin{aligned} Z_1 &= a/2\cos(\theta - \phi - \psi)/2 + b/2\cos(\theta + \phi - \psi)/2, \\ Z_2 &= a/2\sin(\theta - \phi - \psi)/2 + b/2\sin(\theta + \phi - \psi)/2, \\ Z_3 &= \sin(\theta + \phi + \psi)/2, \\ Z_4 &= \cos(\theta + \phi + \psi)/2. \end{aligned} \tag{2.7}$$

From Eq.(2.7), it can be seen that the coordinates, Z_i, satisfy the following equations:

$$Z_1^2 + Z_2^2 = a^2/4 + b^2/4 + (ab/2)\cos(\phi). \tag{2.8}$$

$$Z_3^2 + Z_4^2 = 1. \tag{2.9}$$

Since the range of $\cos(\phi)$ is [-1 1], Eq.(2.8) can be reduced to:

$$(a - b)^2/4 \leq Z_1^2 + Z_2^2 \leq (a + b)^2/4. \tag{2.10}$$

The variables θ and ψ can be eliminated from Eq.(2.7) to yield the following equation:

$$4Z_1^2 + 4Z_2^2 - Z_3^2(a^2 + b^2 + 2ab\cos\phi) - Z_4^2(a^2 + b^2 + 2ab\cos\phi) = 0 \quad (2.11)$$

$a^2 + b^2 + 2ab\cos\phi$ is the square of the distance between the base joint and third joint. Let it be denoted by R. Thus the equation becomes:

$$Z_1^2 + Z_2^2 - \frac{R^2}{4}Z_3^2 - \frac{R^2}{4}Z_4^2 = 0 \quad (2.12)$$

Let the points of R^4 be denoted x=(x,y,z,w) so the above equation can be written as:

$$x^2 + y^2 - \frac{R^2}{4}z^2 - \frac{R^2}{4}w^2 = 0 \quad (2.13)$$

This can be written in the quadratic form as:

$$x^T[Q]x = 0 \quad (2.14)$$

with the coefficient matrix as:

$$Q = \begin{bmatrix} 1 & 0 & 0 & 0 \\ 0 & 1 & 0 & 0 \\ 0 & 0 & -\frac{R^2}{4} & 0 \\ 0 & 0 & 0 & -\frac{R^2}{4} \end{bmatrix} \tag{2.15}$$

As shown in the Figure 2.4 a general choice of fixed and moving reference planes transforms the coefficient matrix to the form below:

$$[Q'] = [C^{-1}]^T [Q][C^{-1}] \tag{2.16}$$

where, $[C] = [G^+][H^-]$ is the matrix form of the quaternion transformation to the new fixed and moving frames.

$$\begin{aligned} [G] &= (x/2, y/2, 0, 1), \\ [H] &= (-x_m/2, -y_m/2, 0, 1) \end{aligned} \tag{2.17}$$

Structure equation for general choice of frames:

$$\mathbf{Y} = \mathbf{GZ}(\theta, \phi, \psi)\mathbf{H}, \tag{2.18}$$

In the matrix form,

$$[Y^T][C^{-1}]^T [Q][C^{-1}][Y] = 0 \tag{2.19}$$

Simplifying we get,

$$F(Z_1, Z_2, Z_3, Z_4) = \frac{(Z_1 - \sigma_1 Z_3 - \tau_1 Z_4)^2 + (Z_2 - \sigma_2 Z_3 - \tau_2 Z_4)^2}{Z_3^2 + Z_4^2}, \text{and} \quad (2.20)$$

$$\begin{aligned} \sigma_1 &= -(y + y_m))/2, \qquad \tau_1 = (x_m - x)/2, \\ \sigma_2 &= (-x_m + x)/2, \qquad \tau_2 = (y - y_m)/2. \end{aligned} \quad (2.21)$$

$$\frac{(a-b)^2}{4} \leq F(Z_1, Z_2, Z_3, Z_4) \leq \frac{(a+b)^2}{4}, \quad (2.22)$$

Eq.(2.22) characterize the kinematic constraints of a planar RRR open chain and define the constraint manifold for the chain.

Thus, the constraint manifold of the planar RRR closed chains is given by a pair of concentric and co-oriented sheared hyperboloid and for the a mechanism to pass through a given motion, the image curve would have to be contained between the constraint manifolds.

Using the projective property of the planar quaternion, to visualize the hyper-geometric shape described by Eq.(2.22), we observe its intersection with the hyperplane $Z_4 = 1$; in the other words, we project Eq.(2.22) onto hyperplane$Z_4 = 1$. Denote $(z_1, z_2, z_3, 1)$ as the projected point of (Z_1, Z_2, Z_3, Z_4), both of which represent the same planar displacement. Then, it is yielded that

$$F(z_1, z_2, z_3, 1) = \frac{(z_1 - \sigma_1 z_3 - \tau_1)^2 + (z_2 - \sigma_2 z_3 - \tau_2)^2}{z_3^2 + 1} \quad (2.23)$$

where σ_1, σ_2, τ_1 and τ_2 are the same as Eq.(2.21).

The volume field described by Eq.(2.23) creates implicit surfaces of (z_1, z_2, z_3). The means to develop the isosurface is to, without loss of generality, set $F(z_1, z_2, z_3, 1) = c$, $c \in [L_{\min}^2/4, L_{\max}^2/4]$, and to be standard, we also reorganize Eq.(2.23) to Eq.(2.24)

$$\frac{(z_1 - \sigma_1 z_3 - \tau_1)^2}{c} + \frac{(z_2 - \sigma_2 z_3 - \tau_2)^2}{c} - z_3^2 = 1 \tag{2.24}$$

This is a typical sheared a circular hyperboloid in the projective (z_1, z_2, z_3) space. See Table 2.2. The hyperboloid centralizes at $(\tau_1, \tau_2, 0)$. The central axis is $\frac{z_1-\tau_1}{\sigma_1} = \frac{z_2-\tau_2}{\sigma_2} = \frac{z_3}{1}$, so that the hyperboloid orients along the vector$(\sigma_1, \sigma_2, 1)$. It is evident to tell that the center and the orientation are decided by the location of the fixed pivot, the length of the floating link and the relative angle of $\mathbf{M}$ to the floating link. Besides, the intersection circle of the hyperboloid with the plane $z_3 = 0$ has a radius, r, equal to $\sqrt{c}$, which determines the size of the hyperboloid; the greater is c, the larger is the size of the hyperboloid. While the value of $F(z_1, z_2, z_3, 1)$ is varying from the lower

Table 2.2: Parameters for the projective sheared hyperboloid presented by equation (2.24)

Geometric Features	Constraint Parameters
Center	$(\tau_1, \tau_2, 0)$
Orientation	$(\sigma_1, \sigma_2, 1)$
Intersected Circle	$\frac{L_{\min}}{2} \leq r = \sqrt{c} \leq \frac{L_{\max}}{2}$

boundary to the ceiling, except that the size of the hyperbolic manifold in-

creases correspondingly, the center and the orientation keep stationary.

The implicit surfaces is a set of concentric and co oriented sheared projective hyperboloid. The hyperboloid set occupies the space bounded by an interior and an exterior hyperboloid in the projective image. Eq.(2.24). A representation of the pair of sheared hyperboloids implemented in Mathematica are shown in Fig. (2.5).

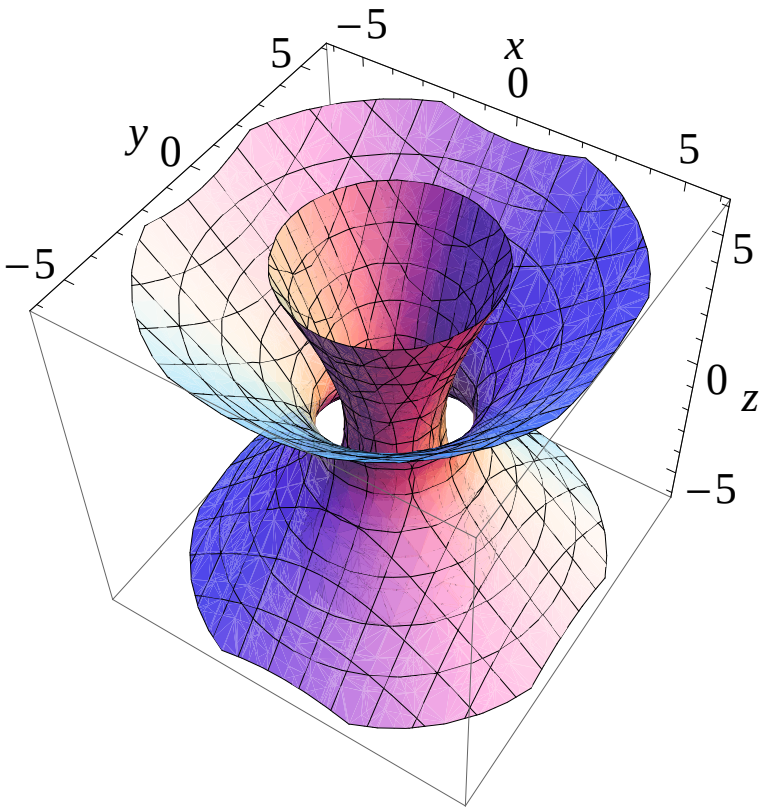

Figure 2.5: A pair of sheared hyperboloids representing a pair of constraint manifolds for an RRR open chain.

2.4.1.1 Inverse Kinematics for Planar RRR Open Chain

The inverse kinematics problem is stated: Given the end-effector pose , calculate the three actuated joint (R or P) values. In the case of an RRR open chain, the joint variables to be calculated are θ, ϕ and ψ. The notations used in the inverse kinematic relations are given below:

A_x, A_y are the $x-$coordinate and $y-$coordinate of point A.
B_x, B_y are the $x-$coordinate and $y-$coordinate of point B.
a, b, and h are the link lengths of first link, second link and coupler link.

$$\begin{aligned} B_x &= X - x_m \cos(\delta) - y_m \sin(\delta), \\ B_y &= Y + y_m \cos(\delta) - x_m \sin(\delta), \end{aligned} \tag{2.25}$$

The length of the coupler is

$$h = \sqrt{(X - B_x)^2 + (Y - B_y)^2} \tag{2.26}$$

and its inclination

$$\alpha = \pi - \tan^{-1}\left(\frac{y_m}{x_m}\right) \tag{2.27}$$

The joint angles can be calculated using the following relations:

$$\theta = \tan^{-1}\left(\frac{(B_x - A_x)^2 + (B_y - A_y)^2 - b^2 - a^2}{2ab}\right) \tag{2.28}$$

$$\phi = \tan^{-1}\left(\frac{B_y - A_y - a\sin(\theta)}{B_x - A_x - a\cos(\theta)}\right) - \theta \tag{2.29}$$

$$\psi = \delta - \alpha - \theta - \phi \tag{2.30}$$

2.4.2 Planar RPR Open Chain

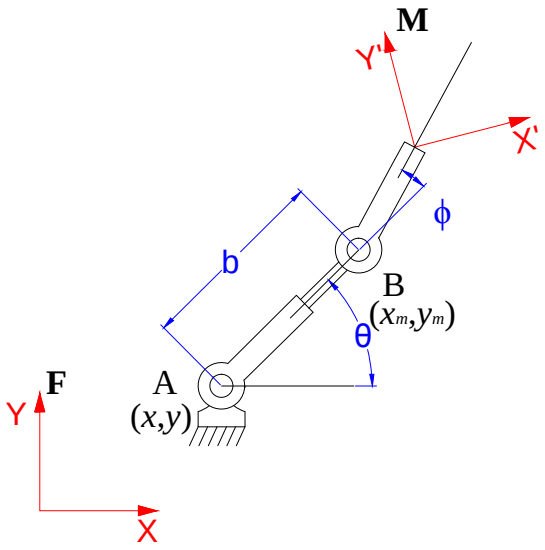

Figure 2.6: A planar RPR open chain

Consider a planar RPR open chain as shown in Fig. 2.6. The length of the first link is b and θ and ϕ are joint angles for two revolute joints respectively. In the figure, **F** and **M** mark the fixed and the moving frames, respectively. The fixed pivot is located at (x, y), while the moving frame is located at (x_m, y_m). When the fixed and moving frames are located at A and B respectively the

parametrized equation of the constraint manifold $\mathbf{Z}(\theta, b, \phi)$ of a RPR open chain is obtained as follows:

$$\mathbf{Z}(\theta, b, \phi) = \mathbf{Z}(\theta)\mathbf{X}(b)\mathbf{Z}(\phi). \tag{2.31}$$

The coordinates of $\mathbf{Z}(\theta, \phi, \psi) = (Z_1, Z_2, Z_3, Z_4)$ can be obtained as:

$$\begin{aligned} Z_1 &= b/2\cos(\theta - \phi)/2, \\ Z_2 &= b/2\sin(\theta - \phi)/2, \\ Z_3 &= \sin(\theta + \phi)/2, \\ Z_4 &= \cos(\theta + \phi)/2. \end{aligned} \tag{2.32}$$

From Eq.(2.32), it can be seen that the coordinates, Z_i, satisfy the following equations:

$$Z_1^2 + Z_2^2 = b^2/4 \tag{2.33}$$

$$Z_3^2 + Z_4^2 = 1. \tag{2.34}$$

Eq.(2.33) we get:

$$b_1^2/4 \leq Z_1^2 + Z_2^2 = b^2/4 \leq b_2^2/4. \tag{2.35}$$

This can be written in the quadratic form as:

$$x^T[Q]x = 0 \tag{2.36}$$

with the coefficient matrix as:

$$Q = \begin{bmatrix} 1 & 0 & 0 & 0 \\ 0 & 1 & 0 & 0 \\ 0 & 0 & 0 & 0 \\ 0 & 0 & 0 & 0 \end{bmatrix} \tag{2.37}$$

As shown in the Fig. (2.6) a general choice of fixed and moving reference planes transforms the coefficient matrix to the form below:

$$[Q'] = [C^{-1}]^T[Q][C^{-1}] \tag{2.38}$$

where, $[C] = [G^+][H^-]$ is the matrix form of the quaternion transformation to the new fixed and moving frames.

$$\begin{aligned} [G] &= (x/2, y/2, 0, 1), \\ [H] &= (-x_m/2, -y_m/2, 0, 1) \end{aligned} \tag{2.39}$$

$$\mathbf{Z}'(\theta, \phi, b)[Q']\mathbf{Z}(\theta, \phi, b) = 0 \tag{2.40}$$

Simplifying the above equation we get:

$$F(Z_1, Z_2, Z_3, Z_4) = \frac{(Z_1 - \sigma_1 Z_3 - \tau_1 Z_4)^2 + (Z_2 - \sigma_2 Z_3 - \tau_2 Z_4)^2}{Z_3^2 + Z_4^2}, \qquad (2.41)$$

where,

$$\begin{aligned} \sigma_1 &= -(y + y_m))/2, \qquad \tau_1 = (x_m - x)/2, \\ \sigma_2 &= (-x_m + x)/2, \qquad \tau_2 = (y - y_m)/2. \end{aligned} \qquad (2.42)$$

$$\frac{b_1^2}{4} \leq F(Z_1, Z_2, Z_3, Z_4) \leq \frac{b_2^2}{4}, \qquad (2.43)$$

Eq.(2.43) characterize the kinematic constraints of a planar RPR open chain and define the constraint manifold for the chain.

Thus, the constraint manifold of the planar RPR closed chains is given by a pair of concentric and co-oriented sheared hyperboloids and for the a mechanism to pass through a given motion, the image curve would have to be contained between the constraint manifolds.

Using the projective property of the planar quaternion, to visualize the hyper-geometric shape described by Eq.(2.43), we observe its intersection with the hyperplane $Z_4 = 1$; in the other words, we project Eq.(2.43) onto hyperplane$Z_4 = 1$. Denote $(z_1, z_2, z_3, 1)$ as the projected point of (Z_1, Z_2, Z_3, Z_4), both of which represent the same planar displacement. Then, it is yielded that

$$F(z_1, z_2, z_3, 1) = \frac{(z_1 - \sigma_1 z_3 - \tau_1)^2 + (z_2 - \sigma_2 z_3 - \tau_2)^2}{z_3^2 + 1} \qquad (2.44)$$

where σ_1, σ_2, τ_1 and τ_2 are the same as Eq.(2.42).

The volume field described by Eq.(2.44) creates implicit surfaces of (z_1, z_2, z_3). The means to develop the isosurface is to, without loss of generality, set $F(z_1, z_2, z_3, 1) = c$, $c \in [L_{\min}^2/4, L_{\max}^2/4]$, and to be standard, we also reorganize Eq.(2.44)

$$\frac{(z_1 - \sigma_1 z_3 - \tau_1)^2}{c} + \frac{(z_2 - \sigma_2 z_3 - \tau_2)^2}{c} - z_3^2 = 1 \tag{2.45}$$

This is a typical sheared a circular hyperboloid in the projective (z_1, z_2, z_3) space. See Table (2.3). The hyperboloid centralizes at $(\tau_1, \tau_2, 0)$. The central axis is $\frac{z_1-\tau_1}{\sigma_1} = \frac{z_2-\tau_2}{\sigma_2} = \frac{z_3}{1}$, so that the hyperboloid orients along the vector$(\sigma_1, \sigma_2, 1)$. It is evident to tell that the center and the orientation are decided by the location of the fixed pivot, the length of the floating link and the relative angle of $\mathbf{M}$ to the floating link. Besides, the intersection circle of the hyperboloid with the plane $z_3 = 0$ has a radius, r, equal to $\sqrt{c}$, which determines the size of the hyperboloid; the greater is c, the larger is the size of the hyperboloid. A representation of the pair of sheared hyperboloids implemented in Mathematica are shown in Fig. (2.7).

2.4.2.1 Inverse Kinematics for Planar RPR Open Chain

The inverse kinematics problem is stated: Given the end-effector pose $\{X, Y, \delta\}^T$, calculate the three actuated joint (R or P) values. In the case of an RPR open chain, the joint variables to be calculated are θ, b and ϕ. The notations used in the inverse kinematic relations are the same as used for the RRR open chain.

Table 2.3: Parameters for the projective sheared hyperboloid presented by Eq.(2.45)

Geometric Features	Constraint Parameters
Center	$(\tau_1, \tau_2, 0)$
Orientation	$(\sigma_1, \sigma_2, 1)$
Intersected Circle	$\frac{L_{\min}}{2} \leq r = \sqrt{c} \leq \frac{L_{\max}}{2}$

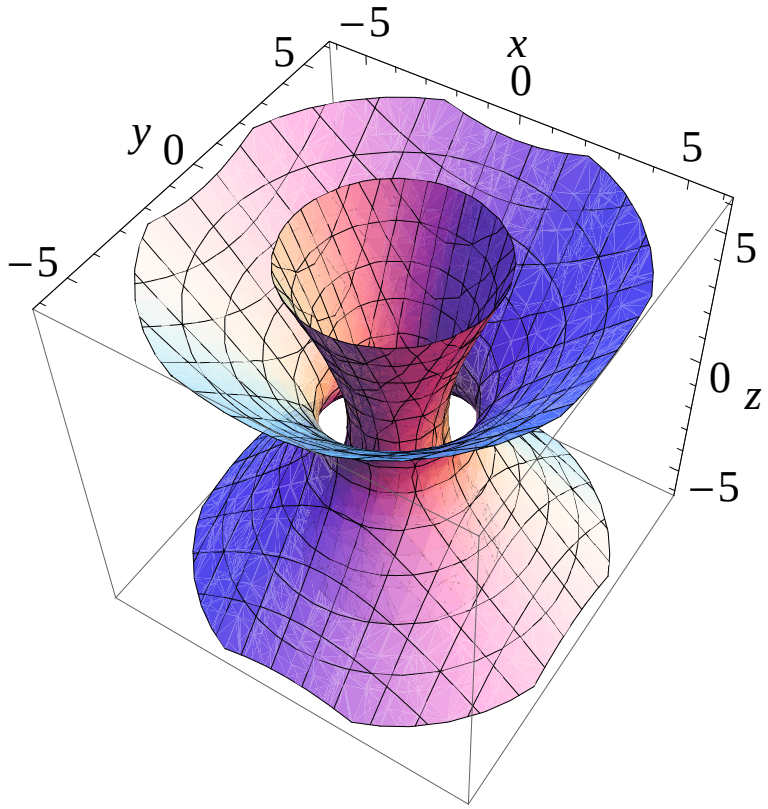

Figure 2.7: A pair of sheared hyperboloids representing a pair of constraint manifolds for an RPR open chain.

The joint angles can be calculated using the following relations:

$$\theta = \tan^{-1}\left(\frac{B_y - A_y}{B_x - A_x}\right) \tag{2.46}$$

$$b = \sqrt{(B_x - A_x)^2 + (B_y - A_y)^2} \tag{2.47}$$

$$\phi = \delta - \alpha - \theta \tag{2.48}$$

2.4.3 Planar RRP Open Chain

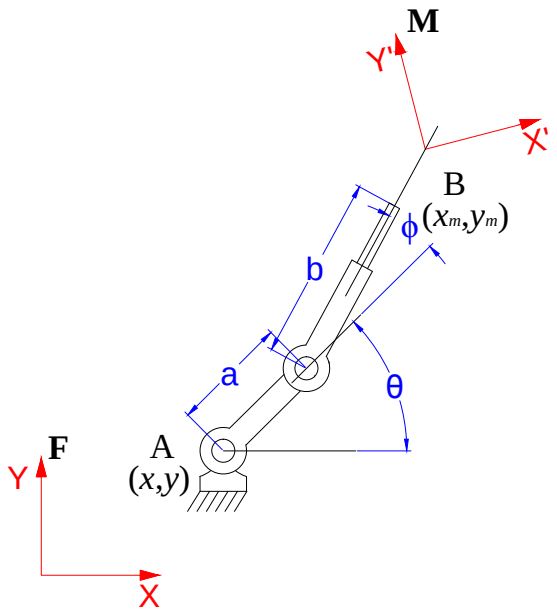

Figure 2.8: A planar RRP open chain

Consider a planar RRP open chain as shown in Fig. (2.8). The length of the first link is a, length of the second link is b and θ and ϕ are joint angles for

two revolute joints respectively. In the figure, **F** and **M** mark the fixed and the moving frames, respectively. The fixed pivot is located at (x, y), while the moving frame is located at (x_m, y_m). When the fixed and moving frames are located at A and B respectively the parametrized equation of the constraint manifold $\mathbf{Z}(\theta, \phi, b)$ of a RRP open chain is obtained as follows:

$$\mathbf{Z}(\theta, b, \phi) = \mathbf{Z}(\theta)\mathbf{X}(a)\mathbf{Z}(\phi)\mathbf{X}(b). \tag{2.49}$$

The coordinates of $\mathbf{Z}(\theta, \phi, b) = (Z_1, Z_2, Z_3, Z_4)$ can be obtained as:

$$\begin{aligned} Z_1 &= b/2\cos(\theta+\phi)/2 + a/2\cos(\theta-\phi)/2, \\ Z_2 &= b/2\sin(\theta+\phi)/2 + a/2\sin(\theta-\phi)/2, \\ Z_3 &= \sin(\theta+\phi)/2, \\ Z_4 &= \cos(\theta+\phi)/2. \end{aligned} \tag{2.50}$$

From Eq.(2.50), it can be seen that the coordinates, Z_i, satisfy the following equations:

$$\tfrac{Z_1 Z_3 - Z_2 Z_4}{Z_3^2 + Z_4^2} = (a/2)\sin(\gamma_b) \in [\tfrac{-a}{2}, \tfrac{a}{2}] \tag{2.51}$$

From Eq.(2.51) we get the quadratic form as:

$$\frac{-a}{2} \leq x^T[Q]x \leq \frac{a}{2}. \tag{2.52}$$

with the coefficient matrix as:

$$Q = \begin{bmatrix} 0 & 0 & 0.5 & 0 \\ 0 & 0 & 0 & -0.5 \\ 0.5 & 0 & -R & 0 \\ 0 & -0.5 & 0 & -R \end{bmatrix} \tag{2.53}$$

As shown in the Fig. (2.8) a general choice of fixed and moving reference planes transforms the coefficient matrix to the form below:

$$[Q'] = [C^{-1}]^T [Q][C^{-1}] \tag{2.54}$$

where, $[C] = [G^+][H^-]$ is the matrix form of the quaternion transformation to the new fixed and moving frames.

$$\begin{aligned} [G] &= (x/2, y/2, 0, 1), \\ [H] &= (-x_m/2, -y_m/2, 0, 1) \end{aligned} \tag{2.55}$$

$$\mathbf{Z}'(\theta, \phi, b)[Q']\mathbf{Z}(\theta, \phi, b) \in [\frac{-a}{2}, \frac{a}{2}] \tag{2.56}$$

Simplifying the above equation we get:

$$(\sigma_1 - R)Z_3^2 + (\tau_2 - R)Z_4^2 + Z_1 Z_3 - xZ_3 Z_4 - Z_2 Z_4 = 0 \tag{2.57}$$

$$\sigma_1 = -(y + y_m)/2, \qquad \tau_2 = (y - y_m)/2. \tag{2.58}$$

$$R \in (\frac{-a}{2}, \frac{a}{2}) \tag{2.59}$$

Eq.(2.59) characterize the kinematic constraints of a planar RRP open chain and define the constraint manifold for the chain.

Thus, the constraint manifold of the planar RRP closed chains is given by a pair of hyperbolic paraboloids and for the a mechanism to pass through a given motion, the image curve would have to be contained in the volume between the constraint manifolds.

Using the projective property of the planar quaternion, to visualize the hyper-geometric shape, we observe its intersection with the hyperplane $Z_4 = 1$; in the other words, we project Eq.(2.57) onto hyperplane $Z_4 = 1$. Denote $(z_1, z_2, z_3, 1)$ as the projected point of (Z_1, Z_2, Z_3, Z_4), both of which represent the same planar displacement. Then, we get

$$\left[Z_3 - \frac{Z_1 - x}{2(R - \sigma_1)}\right]^2 - \left[\frac{Z_1 - x}{2(R - \sigma_1)}\right]^2 = -\left[\frac{(Z_2 + R - \tau_2)}{(R - \sigma_1)}\right] \tag{2.60}$$

This is a typical hyperbolic paraboloid in the projective (z_1, z_2, z_3) space. See Table (2.4). The saddle point of the hyperbolic paraboloid is located at $(x, \tau_2 - R, 0)$. The central axis is $(0, 1, 0)$, so that the hyperbolic paraboloid orients along the $y-$ direction. A representation of the pair of sheared hyperbolic

paraboloids implemented in Mathematica are shown in Fig. (2.9).

As it can be referred from the parameters extracted from the standard equation of a hyperbolic paraboloid, it does not yield all the geometric parameters independently. Hence, in addition to the existing geometric parameters of location of the saddle point and the orientation, we need to define an addition geometric parameter. For a hyperbolic paraboloid the mean curvature of the surfaces at the saddle point yields σ_2. The mean curvature (H) is derived as follows:

$$H(u,v) = \frac{K_1(u,v) + K_2(u,v)}{2}, \tag{2.61}$$

where $K_1(u,v)$ and $K_2(u,v)$ are defined as principal curvatures of the surface at parameters (u,v). From the above Eq.(2.61), the differential form is;

$$H = \frac{1}{2}(\frac{EN - 2MF + GL}{EG - F^2}), \tag{2.62}$$

where E, F, G are the coefficients of the first fundamental form and L, M, N are the coefficients of the second fundamental form.

From the above differential Eq.(2.62), we get:

$$H = R - \sigma_1. \tag{2.63}$$

Table 2.4: Parameters for the projective sheared hyperbolic paraboloid presented by Eq.(2.60)

Geometric Features	Constraint Parameters
Saddle point	$(x, \tau_2 - R, 0)$
Mean curvature	$R - \sigma_1$
Boundaries	$R \in \left[\frac{-a}{2}, \frac{a}{2}\right]$

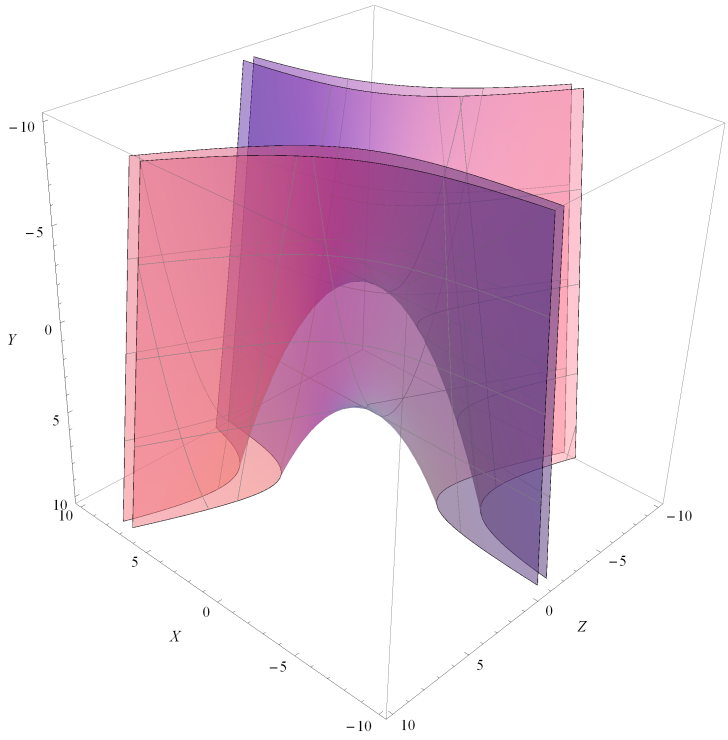

Figure 2.9: A pair of hyperbolic paraboloids representing a pair of constraint manifolds for a RRP open chain.

2.4.3.1 Inverse Kinematics for Planar RRP Open Chain

The inverse kinematics problem is stated: Given the end-effector pose $\{X, Y, \delta\}^T$, calculate the three actuated joint (R or P) values. In the case of an RRP open

chain, the joint variables to be calculated are θ, b and ϕ. The notations used in the inverse kinematic relations are the same as used for the RRR open chain. The joint angles can be calculated using the following relations:

$$\theta = \tan^{-1}\left(\frac{B_y - A_y - b\sin(\delta - \alpha)}{B_x - A_x - b\cos(\delta - \alpha)}\right) \tag{2.64}$$

where, $\alpha = \pi - \tan^{-1}\left(\frac{y_m}{x_m}\right)$

$$b = \left(\frac{-m + \sqrt{m^2 - 4n}}{2}\right) \tag{2.65}$$

where,

$m = -(2(B_x - A_x)\cos(\delta - \alpha) + 2(B_y - A_y)\sin(\delta - \alpha)$

$n = (B_x - A_x)^2 + (B_y - A_y)^2 - a^2$

$$\phi = \delta - \alpha - \theta \tag{2.66}$$

2.4.4 Planar PRR Open Chain

Consider a planar PRR open chain as shown in Fig. (2.10). The length of the first link is a, length of the second link is b and θ and ϕ are joint angles for two revolute joints respectively. In the figure, **F** and **M** mark the fixed and the moving frames, respectively. The fixed pivot is located at (x, y), while the moving frame is located at (x_m, y_m). When the fixed and moving frames are located at A and B respectively the parametrized equation of the constraint manifold $\mathbf{Z}(a, \theta, \phi)$ of a PRR open chain is obtained as follows:

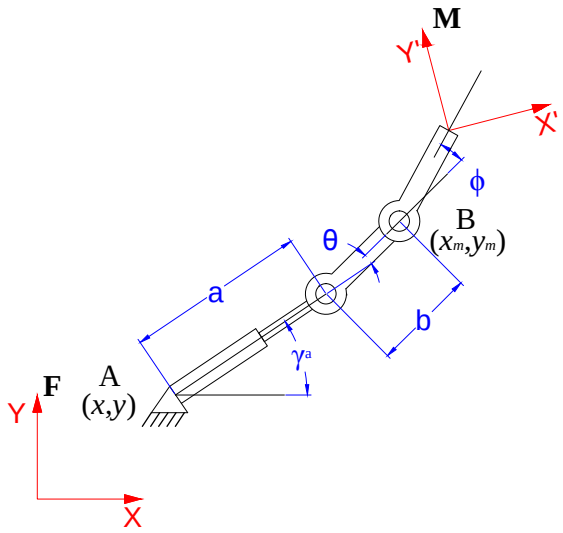

Figure 2.10: A planar PRR open chain

$$\mathbf{Z}(a,\theta,\phi) = \mathbf{X}(a)\mathbf{Z}(\theta)\mathbf{X}(b)\mathbf{Z}(\phi). \tag{2.67}$$

The coordinates of $\mathbf{Z}(a,\theta,\phi) = (Z_1, Z_2, Z_3, Z_4)$ can be obtained as:

$$\begin{aligned} Z_1 &= a/2\cos(\theta+\phi)/2 + b/2\cos(\theta-\phi)/2, \\ Z_2 &= a/2\sin(\theta+\phi)/2 + b/2\sin(\theta-\phi)/2, \\ Z_3 &= \sin(\theta+\phi)/2, \\ Z_4 &= \cos(\theta+\phi)/2. \end{aligned} \tag{2.68}$$

From Eq.(2.68), it can be seen that the coordinates, Z_i, satisfy the following equations:

$$\frac{Z_1 Z_3 + Z_2 Z_4}{Z_3^2 + Z_4^2} = (b/2)\sin(\gamma_a) \tag{2.69}$$

From Eq.(2.69) we can see that the equation is very similar to that for RRP configuration, also we get the quadratic form as:

$$\frac{-b}{2} \leq x^T[Q]x \leq \frac{b}{2}. \tag{2.70}$$

with the coefficient matrix as:

$$Q = \begin{bmatrix} 0 & 0 & 0.5 & 0 \\ 0 & 0 & 0 & 0.5 \\ 0.5 & 0 & -R & 0 \\ 0 & 0.5 & 0 & -R \end{bmatrix} \tag{2.71}$$

As shown in the Fig. (2.10) a general choice of fixed and moving reference planes transforms the coefficient matrix to the form below:

$$[Q'] = [C^{-1}]^T[Q][C^{-1}] \tag{2.72}$$

where, $[C] = [G^+][H^-]$ is the matrix form of the quaternion transformation to the new fixed and moving frames.

$$[G] = (x/2, y/2, 0, 1), \tag{2.73}$$
$$[H] = (-x_m/2, -y_m/2, 0, 1)$$

$$\mathbf{Z}'(a,\theta,\phi)[Q']\mathbf{Z}(a,\theta,\phi) \in (\frac{-b}{2},\frac{b}{2}) \tag{2.74}$$

Simplifying the above equation we get:

$$(\sigma_1 - R)Z_3^2 + (\tau_2 + R)Z_4^2 + Z_1Z_3 + x_mZ_3Z_4 + Z_2Z_4 = 0 \tag{2.75}$$

where,

$$\sigma_1 = -(y + y_m))/2, \qquad \tau_2 = (y - y_m)/2. \tag{2.76}$$

$$R \in (\frac{-b}{2},\frac{b}{2}) \tag{2.77}$$

Eq.(2.75) characterize the kinematic constraints of a planar PRR open chain and define the constraint manifold for the chain.

Thus, the constraint manifold of the planar PRR closed chains is given by a pair of hyperbolic paraboloids and for the a mechanism to pass through a given motion, the image curve would have to be contained in the volume between the constraint manifolds.

Using the projective property of the planar quaternion, to visualize the hyper-geometric shape described by Eq.(2.75), we observe its intersection with the hyperplane $Z_4 = 1$; in the other words, we project Eq.(2.75) onto hyper-plane $Z_4 = 1$. Denote $(z_1, z_2, z_3, 1)$ as the projected point of (Z_1, Z_2, Z_3, Z_4),

both of which represent the same planar displacement. Then,we get

$$\left[Z_3 + \frac{Z_1 + x_m}{2(\sigma_1 - R)}\right]^2 - \left[\frac{Z_1 + x_m}{2(\sigma_1 - R)}\right]^2 = -\left[\frac{(Z_2 - (R - \tau_2))}{(\sigma_1 - R)}\right] \tag{2.78}$$

This is a typical hyperbolic paraboloid in the projective (z_1, z_2, z_3) space. See Table (2.5). The saddle point of the hyperbolic paraboloid is located at $(-x_m, \tau_2 + R, 0)$. The central axis is $(0, 1, 0)$, so that the hyperbolic paraboloid orients along the $y-$ direction. A representation of the pair of sheared hyperbolic paraboloids implemented in Mathematica are shown in Fig. (2.11).

As it can be referred from the parameters extracted from the standard equation of a hyperbolic paraboloid, it does not yield all the geometric parameters independently. Hence, in addition to the existing geometric parameters of location of the saddle point and the orientation, we need to define an addition geometric parameter. For a hyperbolic paraboloid the mean curvature of the surfaces, (H) is derived using the equations (2.61 and 2.62), and we get

$$H = \sigma_1 - R \tag{2.79}$$

2.4.4.1 Inverse Kinematics for Planar PRR Open Chain

The inverse kinematics problem is stated: Given the end-effector pose $\{X, Y, \delta\}^T$, calculate the three actuated joint (R or P) values. In the case of an PRR open chain, the joint variables to be calculated are a, θ and ϕ. The notations used in the inverse kinematic relations are the same as used for the RRR open chain.

Table 2.5: Parameters for the projective sheared hyperbolic paraboloid presented by Eq.(2.78)

Geometric Features	Constraint Parameters
Saddle point	$(-x_m, \tau_2 + R, 0)$
Mean curvature	$-\sigma_1 - R$
Boundaries	$R \in \left[\frac{-b}{2}, \frac{b}{2}\right]$

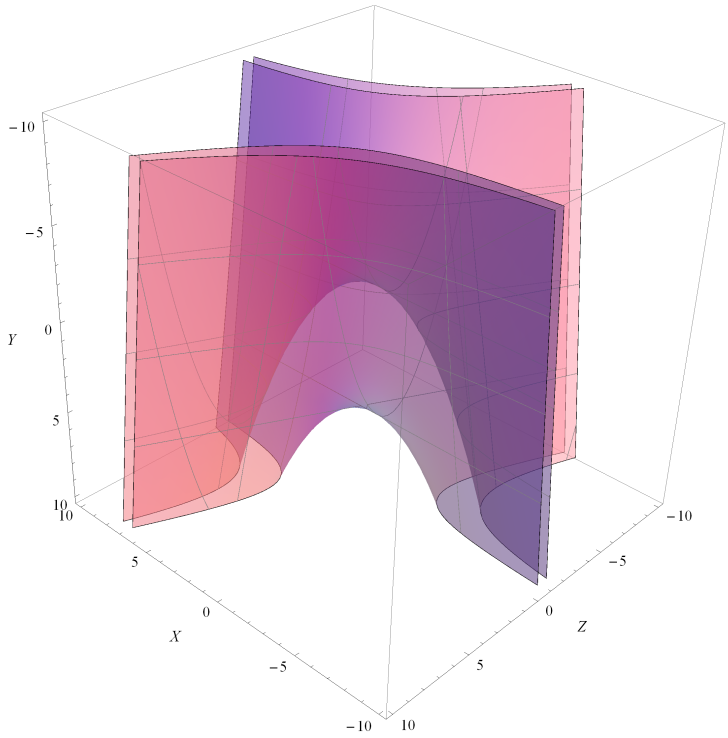

Figure 2.11: A pair of hyperbolic paraboloids representing a pair of constraint manifolds for a PRR open chain.

The joint angles can be calculated using the following relations:

$$\theta = -\gamma_a + \tan^{-1}\left(\frac{B_y - A_y - a\sin(\gamma_a)}{B_x - A_x - a\cos(\gamma_a)}\right) \tag{2.80}$$

$$a = \left(\frac{-m + \sqrt{m^2 - 4n}}{2} \right) \tag{2.81}$$

where,

$m = -2[(B_x - A_x)\cos(\gamma_a) + (B_y - A_y)\sin(\gamma_a)]$

$n = (B_x - A_x)^2 + (B_y - A_y)^2 - b^2$

$$\phi = \delta - \alpha - \theta \tag{2.82}$$

where, $\alpha = \pi - \tan^{-1}\left(\frac{y_m}{x_m}\right)$

2.4.5 Planar PRP Open Chain

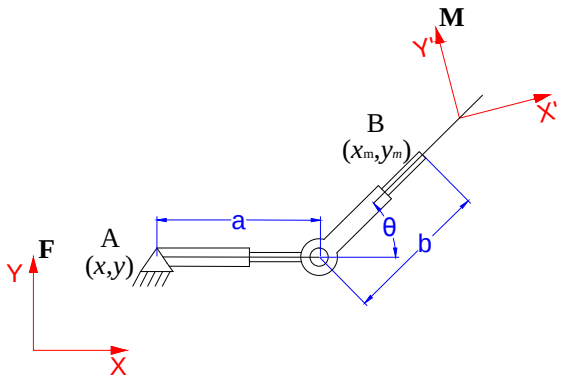

Figure 2.12: A planar PRP open chain

Consider a planar PRP open chain as shown in Fig. 2.12. The length of the first link is a, length of the second link is b and θ is the joint angle for the revolute joint. In the figure, **F** and **M** mark the fixed and the moving frames, respectively. The fixed pivot is located at (x, y), while the moving frame is

located at (x_m, y_m). When the fixed and moving frames are located at A and B respectively the parametrized equation of the constraint manifold $\mathbf{Z}(a, \theta, b)$ of a PRP open chain is obtained as follows:

$$\mathbf{Z}(a, \theta, b) = \mathbf{X}(a)\mathbf{Z}(\theta)\mathbf{X}(b). \tag{2.83}$$

The coordinates of $\mathbf{Z}(a, \theta, b) = (Z_1, Z_2, Z_3, Z_4)$ can be obtained as:

$$\begin{aligned} Z_1 &= (a+b)/2\cos(\theta)/2, \\ Z_2 &= (b-a)/2\sin(\theta)/2, \\ Z_3 &= \sin(\theta)/2, \\ Z_4 &= \cos(\theta)/2. \end{aligned} \tag{2.84}$$

From Eq.(2.84), it can be seen that the coordinates, Z_i, satisfy the following equations:

$$\tfrac{Z_1 Z_3 - Z_2 Z_4}{Z_4 Z_3} \in [a_1, a_2] \tag{2.85}$$

From Eq.(2.85) we can see that the equation is very similar to that for RRP configuration, also we get the quadratic form as:

$$a_1 \leq x^T[Q]x \leq a_2. \tag{2.86}$$

with the coefficient matrix as:

$$Q = \begin{bmatrix} 0 & 0 & 0.5 & 0 \\ 0 & 0 & 0 & -0.5 \\ 0.5 & 0 & 0 & -0.5a \\ 0 & -0.5 & -0.5a & 0 \end{bmatrix} \tag{2.87}$$

As shown in the Fig. (2.12) a general choice of fixed and moving reference planes transforms the coefficient matrix to the form below:

$$[Q'] = [C^{-1}]^T [Q][C^{-1}] \tag{2.88}$$

where, $[C] = [G^+][H^-]$ is the matrix form of the quaternion transformation to the new fixed and moving frames.

$$\begin{aligned} [G] &= (x/2, y/2, 0, 1), \\ [H] &= (-x_m/2, -y_m/2, 0, 1) \end{aligned} \tag{2.89}$$

$$\mathbf{Z}'(a, \theta, b)[Q']\mathbf{Z}(a, \theta, b) \in [a_1, a_2] \tag{2.90}$$

Simplifying the above equation we get:

$$\sigma_1 Z_3^2 + \tau_2 Z_4^2 + Z_1 Z_3 - (x + a) Z_3 Z_4 - Z_2 Z_4 = 0 \tag{2.91}$$

where

$$\sigma_1 = -(y + y_m))/2 \qquad \tau_2 = (y - y_m)/2. \tag{2.92}$$

$$R \in [a_1, a_2] \tag{2.93}$$

Eq.(2.91) characterize the kinematic constraints of a planar PRP open chain and define the constraint manifold for the chain.

Thus, the constraint manifold of the planar PRP closed chains is given by a pair of hyperbolic paraboloids and for the a mechanism to pass through a given motion, the image curve would have to be contained in the volume between the constraint manifolds.

Using the projective property of the planar quaternion, to visualize the hyper-geometric shape described by Eq.(2.91) , we observe its intersection with the hyperplane $Z_4 = 1$; in the other words, we project Eq.(2.91) onto hyperplane $Z_4 = 1$. Denote $(z_1, z_2, z_3, 1)$ as the projected point of (Z_1, Z_2, Z_3, Z_4), both of which represent the same planar displacement. Then,we get

$$\left[Z_3 + \frac{Z_1 - (x + a)}{2\sigma_1}\right]^2 - \left[\frac{Z_1 + (x + a)}{2\sigma_1}\right]^2 = -\left[\frac{(Z_2 - \tau_2)}{2\sigma_1}\right] \tag{2.94}$$

This is a typical hyperbolic paraboloid in the projective (z_1, z_2, z_3) space. See Table (2.6). The saddle point of the hyperbolic paraboloid is located at $(a+x, \tau_2, 0)$. The central axis is $(0, 1, 0)$, so that the hyperbolic paraboloid orients along the $y-$ direction. A representation of the pair of sheared hyperbolic

paraboloids implemented in Mathematica are shown in Fig. (2.13).

As it can be referred from the parameters extracted from the standard equation of a hyperbolic paraboloid, it does not yield all the geometric parameters independently. Hence, in addition to the existing geometric parameters of location of the saddle point and the orientation, we need to define an addition geometric parameter. For a hyperbolic paraboloid the mean curvature of the surfaces at the saddle point yields σ_1. The mean curvature (H) is derived using the equations (2.61 and 2.62), and we get

$$H = -\sigma_1. \tag{2.95}$$

Table 2.6: Parameters for the projective sheared hyperbolic paraboloid presented by Eq.(2.94)

Geometric Features	Constraint Parameters
Saddle point	$(a + x, \tau_2, 0)$
Mean curvature	$-\sigma_1$
Boundaries	$a \in [a_1, a_2]$

2.4.5.1 Inverse Kinematics for Planar PRP Open Chain

The inverse kinematics problem is stated: Given the end-effector pose $\{X, Y, \delta\}^T$, calculate the three actuated joint (R or P) values. In the case of an PRP open chain, the joint variables to be calculated are θ, a and b. The notations used in the inverse kinematic relations are the same as used for the RRR open chain.

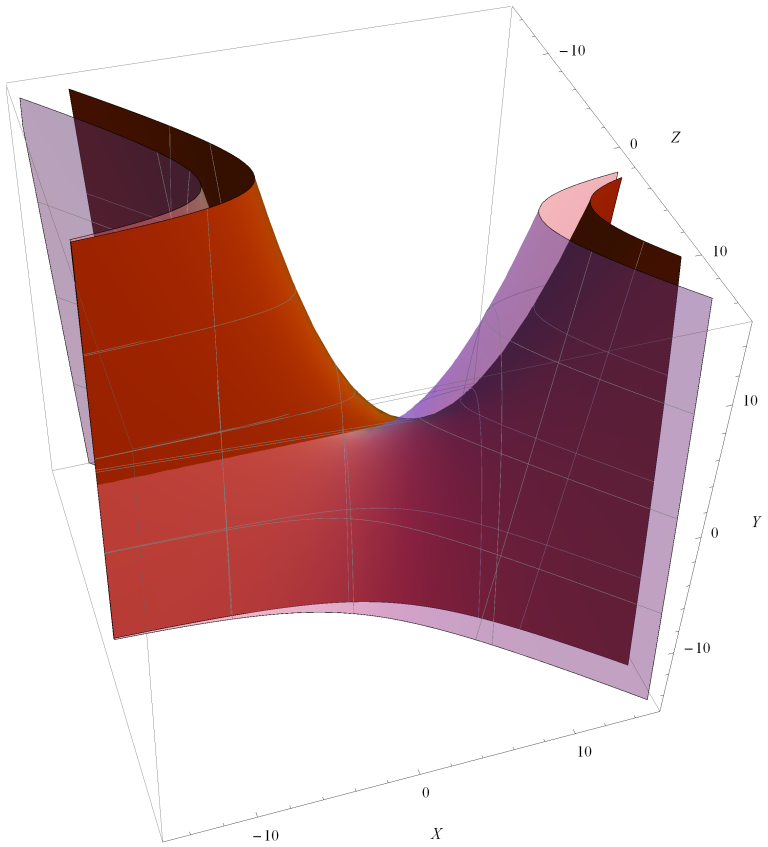

Figure 2.13: A pair of hyperbolic paraboloids representing a pair of constraint manifolds for a PRP open chain.

The joint angles can be calculated using the following relations:

$$a = \frac{(B_x - A_x)\sin(\theta) - (B_y - A_y)\cos(\theta)}{\sin(\theta)} \tag{2.96}$$

$$b = \frac{(B_y - A_y)\cos(\theta)}{\sin(\theta)} \tag{2.97}$$

$$\theta = \delta - \alpha \tag{2.98}$$

where, $\alpha = \pi - \tan^{-1}\left(\frac{y_m}{x_m}\right)$

2.4.6 Planar PPR Open Chain

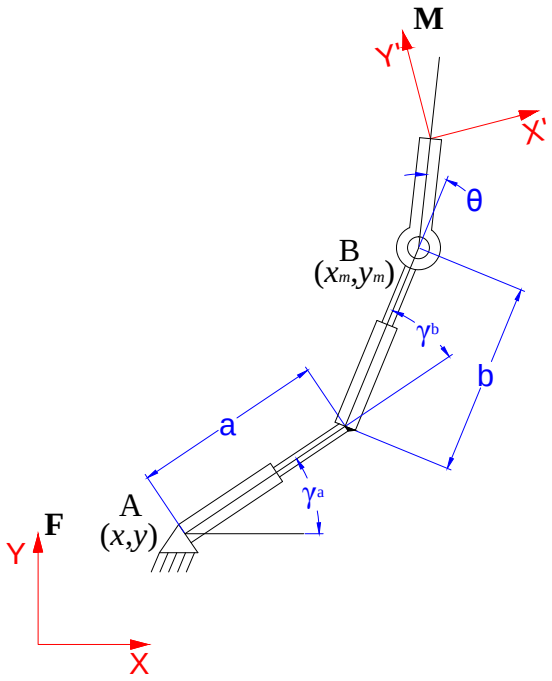

Figure 2.14: A planar PPR open chain

Consider a planar PPR open chain as shown in Fig. (2.14). The length of the first link is a, length of the second link is b, and their inclination angles are γ_a and γ_b respectively and θ is the joint angle for the revolute joint. In the figure, **F** and **M** mark the fixed and the moving frames, respectively. The fixed pivot is located at (x, y), while the moving frame is located at (x_m, y_m) .When the fixed and moving frames are located at A and B respectively the parametrized equation of the constraint manifold $\mathbf{Z}(a, b, \theta)$ of a PPR open

chain is obtained as follows:

$$\mathbf{Z}(a,b,\theta) = \mathbf{Z}(\gamma_a)\mathbf{X}(a)\mathbf{Z}(\gamma_b)\mathbf{X}(b)\mathbf{Z}(\theta). \tag{2.99}$$

The coordinates of $\mathbf{Z}(a,b,\theta) = (Z_1, Z_2, Z_3, Z_4)$ can be obtained as:

$$\begin{aligned} Z_1 &= a/2\cos(\gamma_a - \gamma_b - \theta)/2 + b/2\cos(\gamma_a + \gamma_b - \theta)/2, \\ Z_2 &= a/2\sin(\gamma_a - \gamma_b - \theta)/2 + b/2\sin(\gamma_a + \gamma_b - \theta)/2, \\ Z_3 &= \sin(\gamma_a + \gamma_b + \theta)/2, \\ Z_4 &= \cos(\gamma_a + \gamma_b + \theta)/2. \end{aligned} \tag{2.100}$$

From Eq.(2.100), it can be seen that the coordinates, Z_i, satisfy the following equations:

$$\tfrac{Z_1 Z_3 + Z_2 Z_4}{Z_3^2 + Z_4^2} = (b/2)\sin(\gamma_b) \in [\tfrac{b_1\cos(\gamma_b)}{2}, \tfrac{b_2\cos(\gamma_b)}{2}] \tag{2.101}$$

From Eq.(2.101) we can see that the equation is very similar to that for PRR configuration, also we get the quadratic form as:

$$\left(\frac{b_1\cos(\gamma_b)}{2}\right) \leq x^T[Q]x \leq \left(\frac{b_2\cos(\gamma_b)}{2}\right) \tag{2.102}$$

with the coefficient matrix as:

$$Q = \begin{bmatrix} 0 & 0 & 0.5 & 0 \\ 0 & 0 & 0 & 0.5 \\ 0.5 & 0 & -R & 0 \\ 0 & 0.5 & 0 & -R \end{bmatrix} \tag{2.103}$$

As shown in the Fig. (2.14) a general choice of fixed and moving reference planes transforms the coefficient matrix to the form below:

$$[Q'] = [C^{-1}]^T [Q][C^{-1}] \tag{2.104}$$

where, $[C] = [G^+][H^-]$ is the matrix form of the quaternion transformation to the new fixed and moving frames.

$$\begin{aligned} [G] &= (x/2, y/2, 0, 1), \\ [H] &= (-x_m/2, -y_m/2, 0, 1) \end{aligned} \tag{2.105}$$

$$\mathbf{Z}'(a, b, \theta)[Q']\mathbf{Z}(a, b, \theta) \in [\frac{b_1 \cos(\gamma_b)}{2}, \frac{b_2 \cos(\gamma_b)}{2}] \tag{2.106}$$

Simplifying the above equation we get:

$$(\sigma_1 - R)Z_3^2 - (R + \tau_2)Z_4^2 + Z_1 Z_3 + x_m Z_3 Z_4 + Z_2 Z_4 = 0 \tag{2.107}$$

where

$$\sigma_1 = -(y + y_m))/2, \qquad \tau_2 = (y - y_m)/2. \tag{2.108}$$

$$R \in [\frac{b_1 \cos(\gamma_b)}{2}, \frac{b_2 \cos(\gamma_b)}{2}] \tag{2.109}$$

Eq.(2.107) characterize the kinematic constraints of a planar PPR open chain and define the constraint manifold for the chain.

Thus, the constraint manifold of the planar PPR closed chains is given by a pair of hyperbolic paraboloids and for the a mechanism to pass through a given motion, the image curve would have to be contained in the volume between the constraint manifolds.

Using the projective property of the planar quaternion, to visualize the hyper-geometric shape described by Eq.(2.107), we observe its intersection with the hyperplane $Z_4 = 1$; in the other words, we project Eq.(2.107) onto hyperplane $Z_4 = 1$. Denote $(z_1, z_2, z_3, 1)$ as the projected point of (Z_1, Z_2, Z_3, Z_4), both of which represent the same planar displacement. Then, we get

$$\left[Z_3 + \frac{Z_1 + x_m}{2(\sigma_1 - R)}\right]^2 - \left[\frac{Z_1 + x_m}{2(\sigma_1 - R)}\right]^2 = -\left[\frac{(Z_2 - (R + \tau_2))}{(\sigma_1 - R)}\right] \tag{2.110}$$

This is a typical hyperbolic paraboloid in the projective (z_1, z_2, z_3) space. See Table (2.7). The saddle point of the hyperbolic paraboloid is located at $(-x_m, \tau_2 + R, 0)$. The central axis is $(0, 1, 0)$, so that the hyperbolic paraboloid orients along the $y-$ direction. It is evident to tell that the location of the sad-

dle point and the mean curvature are decided by the location of the fixed pivot, the length of the floating link and the relative angle of **M** to the floating link. A representation of the pair of sheared hyperbolic paraboloids implemented in Mathematica are shown in Fig. (2.15).

As it can be referred from the parameters extracted from the standard equation of a hyperbolic paraboloid, it does not yield all the geometric parameters independently. Hence, in addition to the existing geometric parameters of center point (saddle point) and the orientation, we need to define an addition geometric parameter. For a hyperbolic paraboloid the mean curvature (H) is derived using the equations (2.61 and 2.62), and we get

$$H = \sigma_1. - R \tag{2.111}$$

Table 2.7: Parameters for the projective sheared hyperbolic paraboloid presented by Eq.(2.110)

Geometric Features	Constraint Parameters
Saddle point	$(-x_m, \tau_2 + R, 0)$
Mean curvature	$\sigma_1 - R$
Boundaries	$R \in [\frac{b_1 \cos(\gamma_b)}{2}, \frac{b_2 \cos(\gamma_b)}{2}]$

2.4.6.1 Inverse Kinematics for Planar PPR Open Chain

The inverse kinematics problem is stated: Given the end-effector pose $\{X, Y, \delta\}^T$, calculate the three actuated joint (R or P) values. In the case of an PPR open

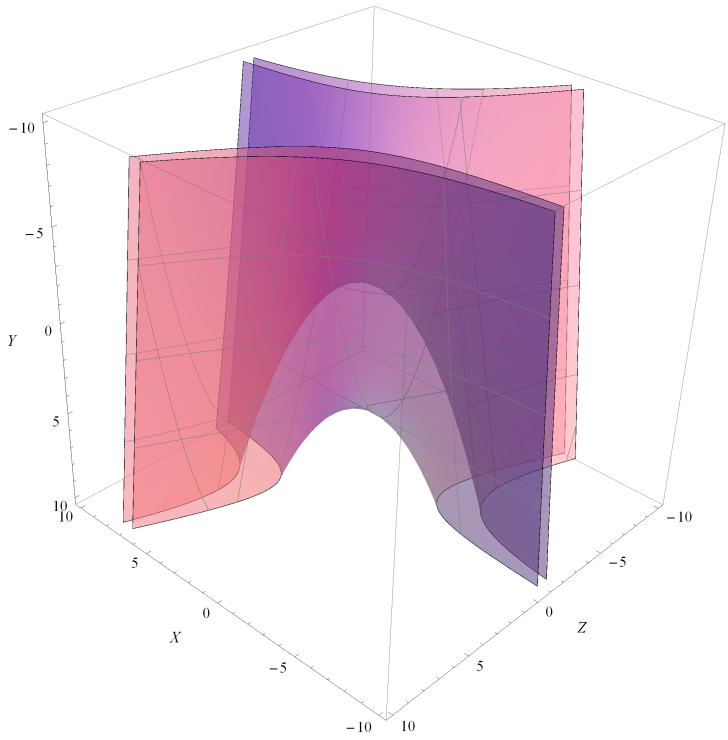

Figure 2.15: A pair of hyperbolic paraboloids representing a pair of constraint manifolds for a PPR open chain.

chain, the joint variables to be calculated are θ, a and b. The notations used in the inverse kinematic relations are the same as used for the RRR open chain. The joint angles can be calculated using the following relations:

$$a = \frac{(B_x - A_x)\sin(\gamma_a + \gamma_b) - (B_y - A_y)\cos(\gamma_a + \gamma_b)}{\sin(\gamma_b)} \tag{2.112}$$

$$b = \frac{-(B_x - A_x)\sin(\gamma_a) + (B_y - A_y)\cos(\gamma_a)}{\sin(\gamma_b)} \tag{2.113}$$

$$\theta = \delta - \alpha \tag{2.114}$$

where, $\alpha = \pi - \tan^{-1}\left(\frac{y_m}{x_m}\right)$

2.4.7 Planar RPP Open Chain

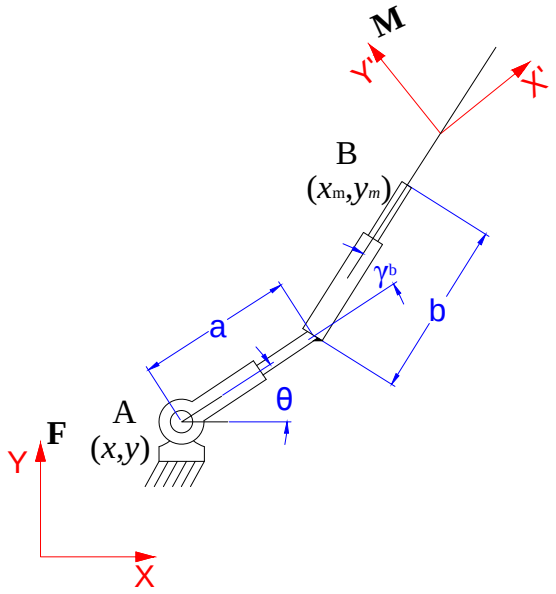

Figure 2.16: A planar RPP open chain

Consider a planar RPP open chain as shown in Fig. (2.16). The length of the first link is a, length of the second link is b, the inclination angle of the second link is γ_b and θ is the joint angle for the revolute joint. In the figure, **F** and **M** mark the fixed and the moving frames, respectively. The fixed pivot is located at (x, y), while the moving frame is located at (x_m, y_m). When the fixed and moving frames are located at A and B respectively the parametrized

equation of the constraint manifold $\mathbf{Z}(\theta, a, b)$ of a RPP open chain is obtained as follows:

$$\mathbf{Z}(\theta, a, b) = \mathbf{Z}(\theta)\mathbf{X}(a)\mathbf{Z}(\gamma_b)\mathbf{X}(b). \tag{2.115}$$

The coordinates of $\mathbf{Z}(\theta, a, b) = (Z_1, Z_2, Z_3, Z_4)$ can be obtained as:

$$\begin{aligned} Z_1 &= a/2\cos(\theta - \gamma_b)/2 + b/2\cos(\theta + \gamma_b)/2, \\ Z_2 &= a/2\sin(\theta - \gamma_b)/2 + b/2\sin(\theta + \gamma_b)/2, \\ Z_3 &= \sin(\theta + \gamma_b)/2, \\ Z_4 &= \cos(\theta + \gamma_b)/2. \end{aligned} \tag{2.116}$$

From Eq.(2.116), it can be seen that the coordinates, Z_i, satisfy the following equations:

$$\frac{Z_1 Z_3 + Z_2 Z_4}{Z_3^2 + Z_4^2} = (a/2)\sin(\gamma_b) \in [\tfrac{a_1 \sin(\gamma_b)}{2}, \tfrac{a_2 \sin(\gamma_b)}{2}] \tag{2.117}$$

From Eq.(2.117) we can see that the equation is very similar to that for RRP configuration, also we get the quadratic form as:

$$\frac{a_1 \sin(\gamma_b)}{2} \leq x^T[Q]x \leq \frac{a_2 \sin(\gamma_b)}{2}. \tag{2.118}$$

with the coefficient matrix as:

$$Q = \begin{bmatrix} 0 & 0 & 0.5 & 0 \\ 0 & 0 & 0 & -0.5 \\ 0.5 & 0 & -R & 0 \\ 0 & -0.5 & 0 & -R \end{bmatrix} \tag{2.119}$$

As shown in the Fig. (2.16) a general choice of fixed and moving reference planes transforms the coefficient matrix to the form below:

$$[Q'] = [C^{-1}]^T [Q][C^{-1}] \tag{2.120}$$

where, $[C] = [G^+][H^-]$ is the matrix form of the quaternion transformation to the new fixed and moving frames.

$$\begin{aligned} [G] &= (x/2, y/2, 0, 1), \\ [H] &= (-x_m/2, -y_m/2, 0, 1) \end{aligned} \tag{2.121}$$

$$\mathbf{Z}'(\theta, a, b)[Q']\mathbf{Z}(\theta, a, b) \in [\frac{a_1 \sin(\gamma_b)}{2}, \frac{a_2 \sin(\gamma_b)}{2}] \tag{2.122}$$

Simplifying the above equation we get:

$$(\sigma_1 - R)Z_3^2 + (\tau_2 - R)Z_4^2 + Z_1 Z_3 - xZ_3 Z_4 - Z_2 Z_4 = 0 \tag{2.123}$$

where,

$$\sigma_1 = -(y + y_m))/2, \qquad \tau_2 = (y - y_m)/2. \tag{2.124}$$

$$R \in [\frac{a_1 \sin(\gamma_b)}{2}, \frac{a_2 \sin(\gamma_b)}{2}] \tag{2.125}$$

Eq.(2.123) characterize the kinematic constraints of a planar RPP open chain and define the constraint manifold for the chain.

Thus, the constraint manifold of the planar RPP closed chains is given by a pair of hyperbolic paraboloids and for the a mechanism to pass through a given motion, the image curve would have to be contained in the volume between the constraint manifolds.

Using the projective property of the planar quaternion, to visualize the hyper-geometric shape described by Eq.(2.123), we observe its intersection with the hyperplane $Z_4 = 1$; in the other words, we project Eq.(2.123) onto hyperplane $Z_4 = 1$. Denote $(z_1, z_2, z_3, 1)$ as the projected point of (Z_1, Z_2, Z_3, Z_4), both of which represent the same planar displacement. Then, we get

$$\left[Z_3 + \frac{Z_1 - x}{2(\sigma_1 - R)}\right]^2 - \left[\frac{Z_1 - x}{2(\sigma_1 - R)}\right]^2 = -\left[\frac{(Z_2 + (R - \tau_2))}{2(\sigma_1 - R)}\right] \tag{2.126}$$

This is a typical hyperbolic paraboloid in the projective (z_1, z_2, z_3) space. See Table (2.8). The saddle point of the hyperbolic paraboloid is located at $(x, \tau_2 - R, 0)$. The central axis is $(0, 1, 0)$, so that the hyperbolic paraboloid orients along the $y-$ direction. A representation of the pair of sheared hyperbolic

paraboloids implemented in Mathematica are shown in Fig. (2.17).

As it can be referred from the parameters extracted from the standard equation of a hyperbolic paraboloid, it does not yield all the geometric parameters independently. Hence, in addition to the existing geometric parameters of center point (saddle point) and the orientation, we need to define an addition geometric parameter. For a hyperbolic paraboloid the mean curvature of the surfaces (H) is derived using the equations (2.61 and 2.62), and we get

$$H = \sigma_1 - R \tag{2.127}$$

Table 2.8: Parameters for the projective sheared hyperbolic paraboloid presented by Eq.(2.126)

Geometric Features	Constraint Parameters
Saddle point	$(x, \tau_2 - R, 0)$
Mean curvature	$\sigma_1 - R$
Boundaries	$R \in [\frac{a_1 \sin(\gamma_b)}{2}, \frac{a_2 \sin(\gamma_b)}{2}]$

2.4.7.1 Inverse Kinematics for Planar RPP Open Chain

The inverse kinematics problem is stated: Given the end-effector pose $\{X, Y, \delta\}^T$, calculate the three actuated joint (R or P) values. In the case of an RPP open chain, the joint variables to be calculated are θ, a and b. The notations used in the inverse kinematic relations are the same as used for the RRR open chain. The joint angles can be calculated using the following relations:

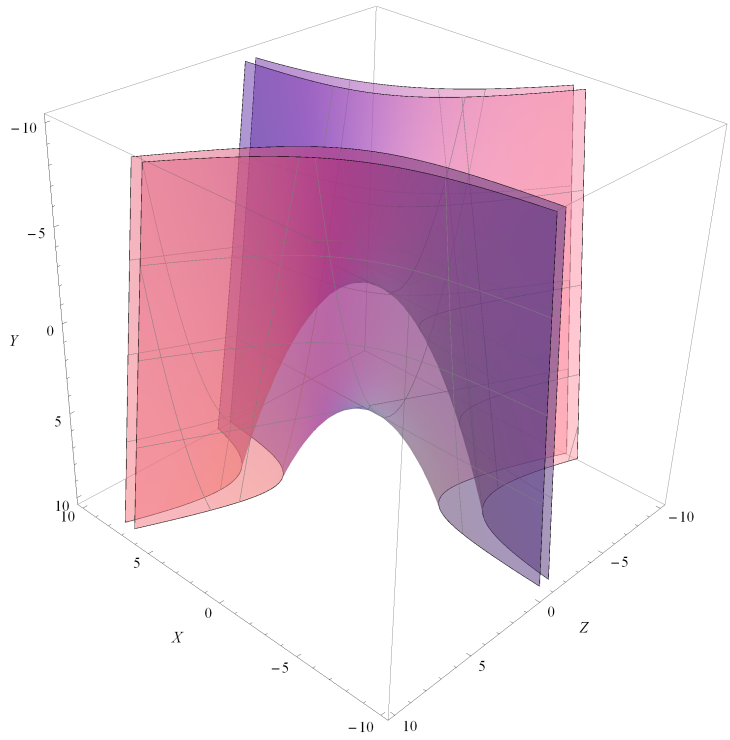

Figure 2.17: A pair of hyperbolic paraboloids representing a pair of constraint manifolds for a RPP open chain.

$$a = \frac{(B_x - A_x)\sin(\gamma_a + \gamma_b) - (B_y - A_y)\cos(\gamma_a + \gamma_b)}{\sin(\gamma_b)} \tag{2.128}$$

$$b = \frac{-(B_x - A_x)\sin(\gamma_a) + (B_y - A_y)\cos(\gamma_a)}{\sin(\gamma_b)} \tag{2.129}$$

$$\theta = \delta - \alpha \tag{2.130}$$

where, $\alpha = \pi - \tan^{-1}\left(\frac{y_m}{x_m}\right)$

2.4.8 A Unifying Representation

Summarizing all the above kinematic constraint equations and the respective constraint manifolds. The constraint manifold for a planar parallel manipulator is the common volume between all the three pairs of surfaces. When the image curve lies inside this common volume, a planar parallel manipulator is designed. Kinematic constraints of all the topologies can be represented by a common uniform equation given below,

$$p_0(Z_1^2+Z_2^2)+p_1Z_3^2+p_2Z_4^2+p_3Z_1Z_3+p_4Z_1Z_4+p_5Z_2Z_3+p_6Z_2Z_4+p_7Z_3Z_4 = 0 \tag{2.131}$$

For RRR- and RPR- chains,

$p_0 = 1$,

$p_7 = \frac{(p_3p_4+p_5p_6)}{2}$

while,for other five RRP-,RPP-,PRR-,PRP-,PPR-chains

$p_0 = 0$,

$p_3 = 1$,

$p_4 = 0$,

$p_5 = 0$,

Table 2.9: Constraint manifold parameters for all the cases

Case	*Center*	*Orientation*	*SkirtRadius*
RRR	$(\tau_1, \tau_2, 0)$	$(\sigma_1, \sigma_2, 1)$	$\frac{\lvert a-b\rvert}{2} \leq R \leq \frac{\lvert a+b\rvert}{2}$
RPR	$(\tau_1, \tau_2, 0)$	$(\sigma_1, \sigma_2, 1)$	$\frac{b_1}{2} \leq R \leq \frac{b_2}{2}$
	SaddlePoint	*MeanCurvature*	*Boundaries*
RRP	$(x, \tau_2 - R, 0)$	$R - \sigma_1$	$R \in [\frac{-a}{2}, \frac{a}{2}]$
PPR	$(-x_m, \tau_2 + R, 0)$	$\sigma_1 - R$	$R \in [\frac{b_1 \cos(\gamma_b)}{2}, \frac{b_2 \cos(\gamma_b)}{2}]$
PRP	$(R + x, \tau_2, 0)$	$-\sigma_1$	$R \in [-a_1, a_2]$
PRR	$(-x_m, \tau_2 + R, 0)$	$-\sigma_1 - R$	$R \in \left[\frac{-b}{2}, \frac{b}{2}\right]$
RPP	$(x, \tau_2 - R, 0)$	$\sigma_1 - R$	$R \in [\frac{a_1 \sin(\gamma_b)}{2}, \frac{a_2 \sin(\gamma_b)}{2}]$

Chapter 3

Object Oriented Software Architecture

3.1 Introduction

This chapter will give an overview of the architecture and describe the top level software components and their interaction.

The software is developed using C++, OpenGL and Qt. It strictly follows an Object Oriented methodology and consist of several sections. The code written is extend-able and re-usable in a way that one just needs to import the definitions of a certain class and can use all the functionalities or methods provided in the class in their own work . In the following section we will discuss some important classes, the functionality they provide and their working.

3.2 Class Design

The kinematic dimensions for an open chain and the associated constraint information is different for every topology.Hence each open chain constitutes a class in the software and has a behavior of its own.Every class has its own unique use which differs completely from other classes. There are other classes,also called helper classes that assist these main classes to achieve certain functionality.

3.2.1 Motion Synthesis class

This class is at a higher level compared to the other classes. It derives from QMainWindow class which is provided by Qt package.It is composed of several other classes like Branch, Motion and Triad and consists of the public slot functions which in-turn invoke the functions of the other classes. Motion Synthesis class contains some important function implementation for saving, reading the motion and contains connections/links to the function of other classes which will be driven by the Graphical User Interface.

3.2.2 Triad class

This is an abstract base class and the characteristic common to all the leg topologies is implemented in here.It contains the definition of set and get function for every leg and contains some other pure virtual functions for inverse kinematics, Cartesian space drawing of mechanism and violation test. Each

derived open chain class has an implementation of its own that contributes to their uniqueness for these functions.

3.2.3 Constraint manifold classes

There are two classes that fall into this category, Hyperboloid and Hyperbolic Paraboloid class. These classes are used for drawing the constraint manifold that's associated with each open chain. These take the input parameters calculated in the open chain classes and use that information for drawing purpose.As each open chain has a manifold associated with it, the constraint manifold class is generally composed within the Open chain class as they share ‘‘has-a" relationship

3.2.4 Open Chain classes

Open chain classes are the leg topolgies that the user selects to design a manipulator.As there are seven topologies,there are seven different classes namely RRR, RPR, RRP, PRR, PRP, PPR, and RPP. Each of these classes consists of a constraint manifold pointer associated with it. For eg. the kinematic constraint surface like Hyperboloid is associated with RRR and RPR, where as Hyperbolic paraboloid is associated with RRP, PRR, PRP, PPR and RPP. Each derived class has its own implementation for Cartesian space visualization, inverse kinematic, violation test and calculation for image space and mechanism parameters.Since all the open chains are triads,they derive from the abstract base class *Triad* as they hold ‘‘Is-a" relationship.Fig.(3.1).

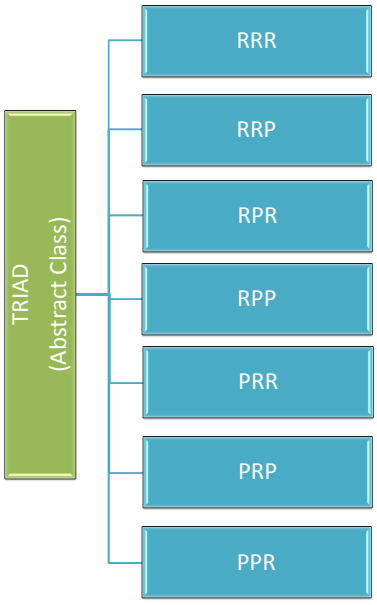

Figure 3.1: Inheritance

Chapter 4

Interactive Dimensional Synthesis

4.1 Design Methodology

The design method treats a three legged planar parallel manipulator as three independent 3-DOF open chains assembled together. The constraint manifold of all the chains are geometric objects in the image space, the size, shape and position of which are a function of the mechanism parameters. A given rational motion maps to an image curve that needs to be contained inside the volume between these constraint manifolds. This section, describes the procedure required to design a planar parallel manipulator. It also describes the user interface with which the designer needs to be familiar with. The basic idea is that the designers are provided with a set of controls via the

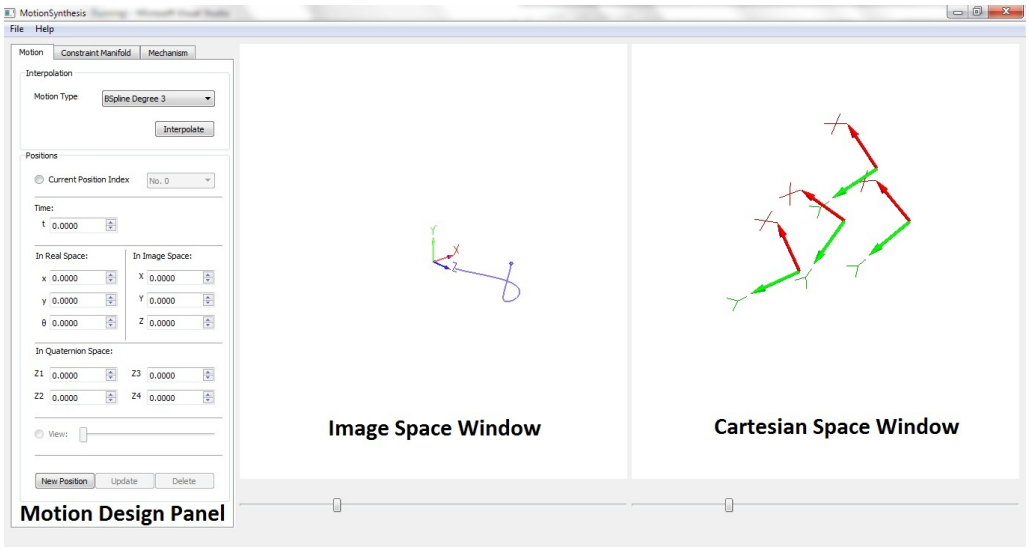

Figure 4.1: A screenshot of the motion design panel and the window spaces

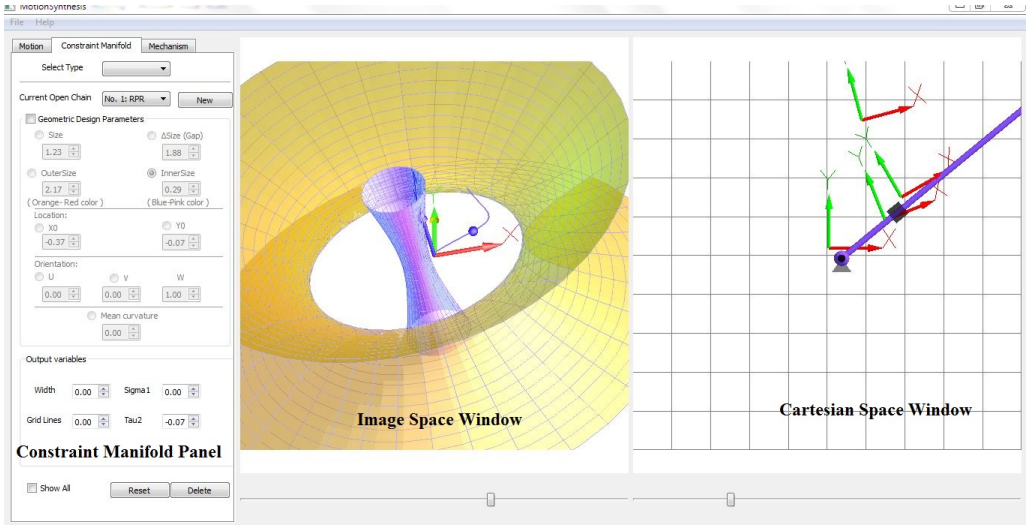

Figure 4.2: A screenshot of the manifold design panel and the window spaces

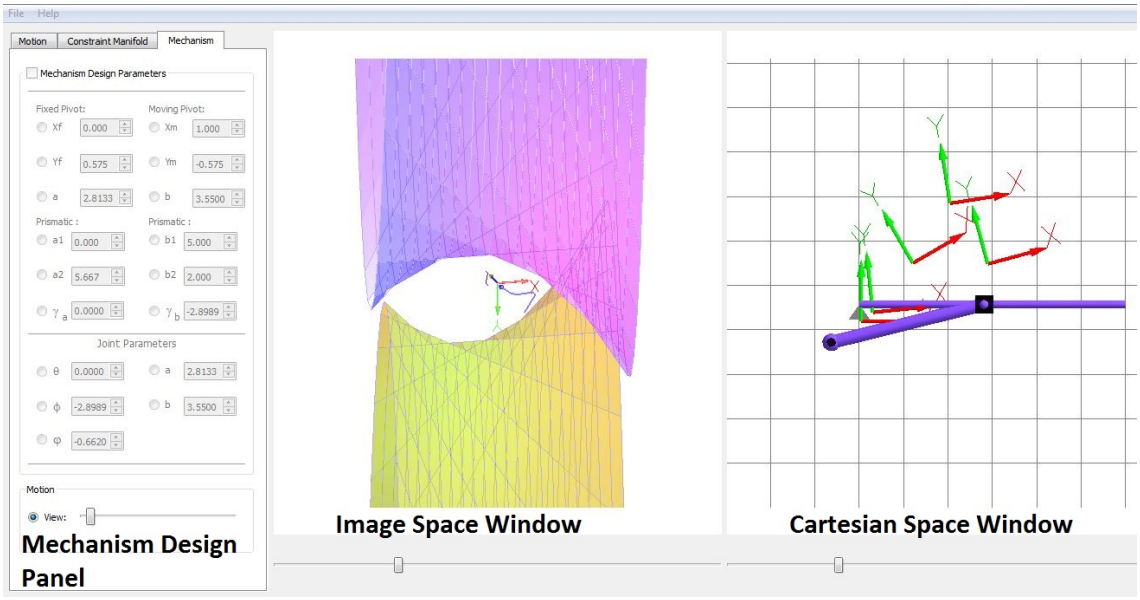

Figure 4.3: A screenshot of the mechanism design panel and the window spaces

graphical user interface (GUI) of the tool that will allow them to interactively manipulate the constraint manifold with the objective to contain the image curve in volume between the pair of constraint manifold.Once that is achieved, the designer will be allowed to instruct the program to check if there are any violations of the kinematic constraints.

4.1.1 User Interface Functionalities

In terms of functionalities, the GUI has following parts and functionalities, as shown in Figs. (4.1), (4.2), and (4.3).

1. The Cartesian Space Window (CSW): This window is used to display the given positions, the animation of the mechanism and the open chains

in the Cartesian space.

2. The Image Space Window (ISW): In this window, the constraint manifold as well as the image curve projected on the hyperplane are shown.

3. Motion Design Panel (MoDP): This panel supports operations like position insertion, deletion and modification, and comprises of functions to animate the motion and to test for constraint violation. The constraint violation test is done and the test results are visualized through the user interface. This operation updates both the Cartesian Space Window and the Image space Window.

4. Constraint Manifold Panel (CoMP): There are two ways to edit the mechanism: 1) directly manipulate mechanism parameters in the Cartesian space, like the location, the link lengths and the relative angle, and as a consequence, constraint manifolds change in the image space, or 2) Edit the geometric parameters that change the size, position, and the orientation of the manifolds.

   This panel allows the user to manipulate the geometric parameters associated with the constraint manifold so as to contain the image curve.This approach is more intuitive.

5. Mechanism Design Panel (MeDP): This panel allows the user to manipulate the mechanism parameters such as location of fixed pivot, link lengths, and relative angles associated with the open chain. The con-

straint violation test is can also be done here and the results are visualized through the user interface. This operation updates both the Cartesian Space Window and the Image space Window.

6. Saving, Reloading and Output : This functionality allows the user to save,reload or output the results or process of designing a manipulator or an open chain.These options can be found under drop down list of File. Once the file is saved using *Save file* feature it allows the user to specify the location of storage and give the flexibility to reload the same file using *Load file* feature.Once the file is loaded,user can resume the task.Once the design is complete,user can get the output mechanism parameters or dimension using *Output file* feature.A text file is generated which specifies the details of the the mechanism/manipulator obtained as a result of designing.

4.2 Design Procedure

1. Use the Motion Design panel to input given positions, associated time parameter, and interpolate them using a NURBS motion.

   The given planar positions can be input with the time parameter t, either using planar quaternion coordinates (Z_1, Z_2, Z_3, Z_4), or Cartesian coordinate directly (x, y, δ). Once all given positions are input, a cubic C^2 B-Spline motion that interpolates the given positions is generated. Consequently, the ISW shows the image points of the prescribed po-

sitions, and renders a continuous NURBS curve which passes through all the image points; while the CSW shows the given positions and the rational motion.

2. Switch to the Constraint Manifold panel. Dimensional synthesis starts with the choice of RRR, RPR, RRP, PRR, PRP, PPR, RPP open chains. The procedure for all the chains is very similar, hence only one open chain is discussed below, exceptions are described:

   In the CSW, initially, the fixed pivots are located at $(x, y) = (0, 0)$; the links have unit length $a_1 = b_1$. In the ISW, a pair of surfaces appear (For RRR and RPR the surface is a hyperboloid, for the rest it is a hyperbolic paraboloid). The default surface pair will be visualized initially. At this point, it will be apparent that the image curve is not completely contained between the pair of surfaces, which means that the constraints are being violated.

3. Modify the constraint manifold visually (for cases PPR and RPP set the orientation of the prismatic joints from MeDP initially, then modify constraint manifold) using the spinner controls (up and down arrows next to parameters) provided in the CoMP until the curve seems completely contained between the two pairs of surfaces. Dragging the slider in either ISW or CSW verifies if the constraints are actually satisfied or not. Using the current value of the mechanism parameters, the program automatically checks the constraint equations if they are satisfied. When

they are satisfied, the program outputs links' length, fixed and moving pivot locations, and the orientation of the moving frame.

4. Repeat steps 2, 3 and 4, and synthesize the other two open chain.

5. Also note there can be several combinations to have a three legged planar parallel manipulator. Each leg can be chosen from the given configurations, *RRR, RPR, RRP, PRR, PRP, PPR, RPP*.

4.3 Example for Planar Parallel Manipulator

In this section, an example is shown that demonstrates the dimensional synthesis of a planar parallel manipulator (RRR, PRR and RRP) using the constraint manifold modification for a given degree six rational motion.

Table 4.1: Cartesian coordinates of four prescribed positions along with their time parameter values

i	x,	y,	$\delta(^\circ)$	u_i
0	0.0448	0.1940	0	0.0
1	1.2067	1.5029	30	0.3
2	2.894	1.4852	15	0.6
3	2.045	2.8478	9	1.0

In this example, we use four positions as given in Table 4.1. The positions are given in Cartesian coordinate (x, y, δ), which specify the location of origin of moving frame $\mathbf{M}$ and the relative angle of $\mathbf{M}$ to horizontal axis of the fixed frame. Also given are the time parameter values (u_i) associated with each

position. First, the given positions are converted to planar quaternion representation (Z_1, Z_2, Z_3, Z_4) and then they are interpolated using a degree six NURBS motion. The image curve is visualized using Rodrigues parameters (see Bottema and Roth [11]) given by $(Z_1/Z_4, Z_2/Z_4, Z_3/Z_4)$. Hereafter, one RRR open chains called A, one PRR open chain called B and one RRP open chain called C and their constraint manifolds are initialized. However, navigating through the motion, it is found that the constraints are violated – this shows up as the image curve being outside the manifold. The designer next modifies the constraint manifolds by varying various geometric parameters interactively. Different parameters have different effect on the size, position, and orientation of the manifold and the process is intuitive. Once the synthesis of three individual open chains A,B and C is completed (see Figs.(4.4), (4.5) and (4.6)), the assembly of A, B and C yields a planar parallel manipulator (see Fig. 4.7) that passes through the given four positions with a continuous motion. Table 4.2 lists the design results.

Table 4.2: Synthesis parameters planar parallel manipulator, example 1

	x	y	a	a_1	a_2	b	b_1	b_2	x_m	y_m
Open Chain A (RRR)	-3.0	-1.8	6.36	-	-	4.64	-	-	5.0	2.0
Open Chain B (PRR)	3.0	0.5	-	0	5.062	5.0	-	-	0.0	0.0
Open Chain C(RRP)	0.0	-3.0	5.0	-	-	-	0.29	7.15	1.0	-1.0

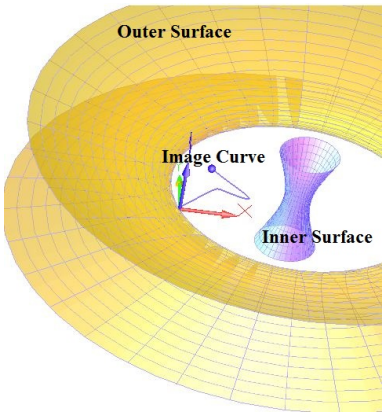

Figure 4.4: Constraint manifold of the RRR Open Chain A and image curve; in this figure, the image curve is completely contained inside the manifold.

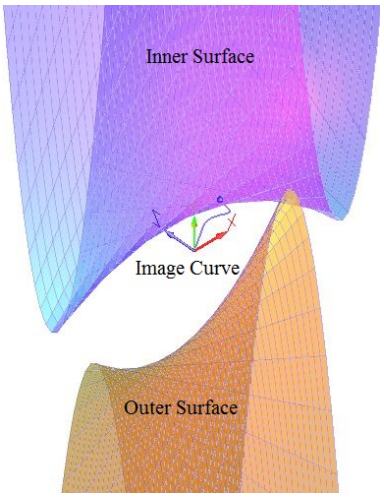

Figure 4.5: Constraint manifold of the PRR Open Chain B and image curve; in this figure, the image curve is completely contained inside the manifold.

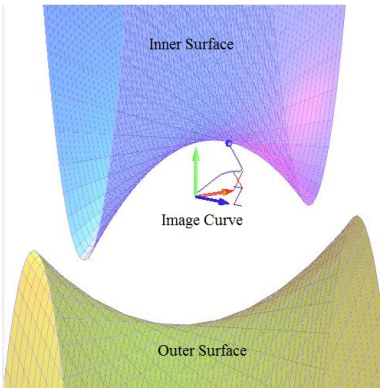

Figure 4.6: Constraint manifold of the RRP Open Chain C and image curve; in this figure, the image curve is completely contained inside the manifold.

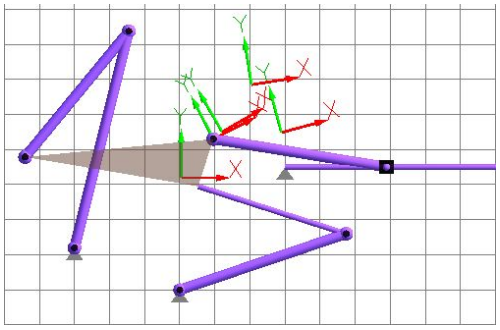

Figure 4.7: Planar parallel manipulator consisting of RRR, PRR, and RRP type legs.

Chapter 5

Algebraic Fitting method for Spherical Four-Bar Linkages

5.1 Introduction

A spherical four-bar mechanism is a closed chain linked by four revolute joins that incidents with one point.In this chapter we discuss the problem of synthesizing a spherical four bar linkage mechanism to realize a set of prescribed positions from the view point of kinematic extraction of geometric constraints from the given motion.The organization of the chapter is as follows.Section 5.2 reviews the concept of kinematic mapping and image space in so far as necessary for the development of this chapter. Section 5.3presents spherical circular geometric constraints associated with spherical dyad motions. Section 5.4 deals with synthesizing the circular constraint with our approach.Further

Section 5.5 discusses about the software developed and the process of designing using an example.

5.2 Spherical Displacement and Quaternion

Any rotation in three-dimensional space has a rotation axis and a rotation angle about this axis. Let $\mathbf{s} = (s_x, s_y, s_z)$ denote a unit vector along the axis and θ denote the angle of rotation. They can be used to define the so-called *Euler-Rodrigues parameters:*

$$q_1 = s_x \sin(\theta/2), q_2 = s_y \sin(\theta/2), q_3 = s_z \sin(\theta/2), q_4 = \cos(\theta/2). \tag{5.1}$$

The Euler-Rodrigues parameters and the quaternion units, $1, \mathbf{i}, \mathbf{j}, \mathbf{k}$ can be combined to define a quaternion of rotation:

$$\mathbf{q} = q_1\mathbf{i} + q_2\mathbf{j} + q_3\mathbf{k} + q_4. \tag{5.2}$$

A quaternion $\mathbf{q}$, at times, is also written as an ordered quadruple (q_1, q_2, q_3, q_4). Since $q_1^2 + q_2^2 + q_3^2 + q_4^2 = 1$, $\mathbf{q}$ is also called a unit quaternion.

If we consider $\mathbf{x}$ and $\mathbf{X}$ as the *vector quaternions* (no coefficient of 1), then the rotation is given by the quaternion equation

$$\mathbf{X} = \mathbf{qxq}^* \tag{5.3}$$

where $\mathbf{q}^* = q_4 - q_1\mathbf{i} - q_2\mathbf{j} - q_3\mathbf{k}$ is the conjugate of $\mathbf{q}$.

We can apply homogeneous transform matrix form to represent the Eq. 5.3:

$$\begin{bmatrix} \mathbf{X} \\ 1 \end{bmatrix} = [R] \begin{bmatrix} \mathbf{x} \\ 1 \end{bmatrix}, \tag{5.4}$$

where

$$[R] = \frac{1}{S^2} \begin{bmatrix} q_4^2 + q_1^2 - q_2^2 - q_3^2 & 2(q_1q_2 - q_4q_3) & 2(q_1q_3 + q_4q_2) \\ 2(q_1q_2 + q_4q_3) & q_4^2 - q_1^2 + q_2^2 - q_3^2 & 2(q_2q_3 - q_4q_1) \\ 2(q_1q_3 - q_4q_2) & 2(q_2q_3 + q_4q_1) & q_4^2 - q_1^2 - q_2^2 + q_3^2 \end{bmatrix}. \tag{5.5}$$

where $S^2 = q_1^2 + q_2^2 + q_3^2 + q_4^2$.

Note that when q_i is replaced by $Q_i = wq_i$ $(i = 1, 2, 3, 4)$, where w is a nonzero scalar, the matrix $[R]$ is unchanged. Thus, the quaternion components of $\mathbf{q}$ can be considered as homogeneous coordinates of a rotation.The four-dimensional vector $q = (q_1, q_2, q_3, q_4)$ is said to define a point in a projective three-dimensional space called the image space of spherical displacement. In this way, a spherical displacement is represented by a point in image space, and a single degree of freedom motion is represented by a curve in image space.

Quaternion algebra is also used for composing two successive rotations. Let $\mathbf{Q}_0, \mathbf{Q}_1$ denote two rotations. The composition of two rotations $\mathbf{Q}_1$ followed by $\mathbf{Q}_0$ is given by the quaternion product $\mathbf{Q}_0\mathbf{Q}_1$.

5.3 Constraints for a Spherical RR Dyad

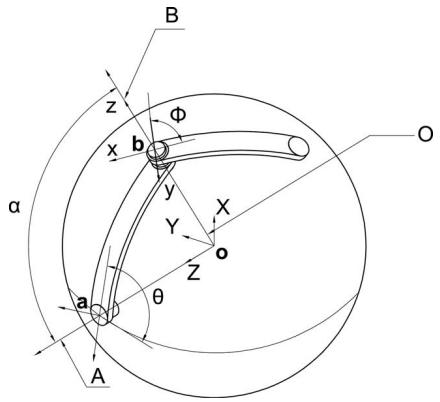

Figure 5.1: A spherical 2R robot arm.

All the mechanisms and motions are considered on the unit sphere, i.e. all the displacements are considered as pure rotations, we can set both fixed frame and moving frame at the origin (center of the unit sphere), while the moving frame rotates with respect to the fixed frame. A spherical RR dyad(Fig. 5.1) can be described as a simple geometric constraint that one of its points on the moving rigid body always traces a circle on the unit sphere. Let (x, y, z) denotes the moving frame coordinates of the point on the moving rigid body, with the rotational matrix in equation 5.5, its homogeneous coordinates (X, Y, Z, W)

in the fixed frame can then be expressed as

$$\begin{aligned} X &= (q_4^2 + q_1^2 - q_2^2 - q_3^2)x + 2(q_1q_2 - q_4q_3)y + 2(q_1q_3 + q_4q_2)z, \\ Y &= 2(q_1q_2 + q_4q_3)x + (q_4^2 - q_1^2 + q_2^2 - q_3^2)y + 2(q_2q_3 - q_4q_1)z, \\ Z &= 2(q_1q_3 - q_4q_2)x + 2(q_2q_3 + q_4q_1)y + (q_4^2 - q_1^2 - q_2^2 + q_3^2)z, \\ W &= q_1^2 + q_2^2 + q_3^2 + q_4^2. \end{aligned} \tag{5.6}$$

where(q_1, q_2, q_3, q_4) is the quaternion that represents the rotation from the fixed frame to the moving frame. Note it is straightforward that if (x, y, z) locates on the unit sphere, i.e., if $x^2 + y^2 + z^2 = 1$ is imposed, (X, Y, Z, W) also lies on the unit sphere. It is obvious that a circle on the unit sphere can be viewed as the intersection of the unit sphere and a plane $aX + bY + cZ + dW = 0$, therefore, now that (X, Y, Z, W) lies on the sphere, we needs to impose the expression of the plane. In other words, as long as (X, Y, Z, W) satisfies $aX + bY + cZ + dW = 0$, given that it already lies on the unit sphere, its trajectory will be a spherical circle, and the spherical center $A = (A_x, A_y, A_z)$ of the circle (as the fixed pivot in Figure. 5.1) locates at:

$$\begin{aligned} A_x &= -\frac{a}{\sqrt{a^2 + b^2 + c^2}}, \\ A_y &= -\frac{b}{\sqrt{a^2 + b^2 + c^2}}, \\ A_z &= -\frac{c}{\sqrt{a^2 + b^2 + c^2}}. \end{aligned} \tag{5.7}$$

and the radius of the circle is denoted by the sphere center angle α:

$$\alpha = |arccos(\frac{d}{\sqrt{a^2+b^2+c^2}})|. \tag{5.8}$$

Now, substitute 5.6 into $aX + bY + cZ + dW = 0$, we obtain a quadric with 10 homogeneous terms:

$$\begin{aligned}
&P_1(q_4^2 + q_1^2 - q_2^2 - q_3^2) + 2P_2(q_1q_2 - q_4q_3) + 2P_3(q_1q_3 + q_4q_2) \\
&+2P_4(q_1q_2 + q_4q_3) + P_5(q_4^2 - q_1^2 + q_2^2 - q_3^2) + 2P_6(q_2q_3 - q_4q_1) \\
&+2P_7(q_1q_3 - q_4q_2) + 2P_8(q_2q_3 + q_4q_1) + P_9(q_4^2 - q_1^2 - q_2^2 + q_3^2) \\
&+P_{10}(q_1^2 + q_2^2 + q_3^2 + q_4^2) = 0.
\end{aligned} \tag{5.9}$$

where

$$\begin{aligned}
&P_1 = ax, \quad P_2 = ay, \quad P_3 = az \\
&P_4 = bx, \quad P_5 = by, \quad P_6 = bz \\
&P_7 = cx, \quad P_8 = cy, \quad P_9 = cz \\
&P_{10} = d.
\end{aligned} \tag{5.10}$$

From the above equation we have 10 homogeneous coefficients but only 7 parameters, furthermore, both a, b, c, d and x, y, z are homogeneous, too. Thus, we should be able to find 4 relationships within those 10 homogeneous coefficients. It can be found that the $10th$ coefficient is independent of the rest,

and the first 9 parameters satisfy the following equations:

$$\begin{aligned} &P_1 : P_2 : P_3 = P_4 : P_5 : P_6, \\ &P_4 : P_5 : P_6 = P_7 : P_8 : P_9, \\ &P_1 : P_2 : P_3 = P_7 : P_8 : P_9. \end{aligned} \tag{5.11}$$

which is equivalent as:

$$\begin{aligned} &P_1P_5 = P_4P_2, P_1P_6 = P_4P_3, P_2P_6 = P_5P_3, \\ &P_4P_8 = P_7P_5, P_4P_9 = P_7P_6, P_5P_9 = P_8P_6, \\ &P_1P_8 = P_7P_2, P_1P_9 = P_7P_3, P_2P_9 = P_8P_3. \end{aligned} \tag{5.12}$$

By observing the above 9 equations, it is not difficult to find that these 9 equations are actually dependent, and only 4 of them, which have to contain all the coefficients from P_1 to P_9, are sufficient and necessary to capture the relations in Eq. 5.11. For example, in this paper we take these four equations to represent 5.11:

$$\begin{aligned} &P_1P_5 - P_4P_2 = 0, P_2P_6 - P_5P_3 = 0, \\ &P_1P_8 - P_7P_2 = 0, P_2P_9 - P_8P_3 = 0. \end{aligned} \tag{5.13}$$

It is easy to derive that the above four equations are equivalent as 5.11 (i.e. the rest five equations in 5.12 can be obtained by these four) except for the case that P_1, P_2 and P_3 are all equal to zero or that P_2, P_5 and P_8 are all equal to zero. However, if $P_1 = P_2 = P_3 = 0$ or $P_2 = P_5 = P_8 = 0$ does appear, then one extra equation is required, which has to exclude these three coefficients.

For example in this paper, we use:

$$P_4P_9 - P_7P_6 = 0 \tag{5.14}$$

To sum up, suppose we are given 10 arbitrary coefficients $\mathbf{P} = \{P_1, P_2, ...P_{10}\}$, they are qualified to be those in 5.10 and hereby utilized to find the parameters a, b, c, d and x, y, z only if they satisfy the four relationships in 5.13, or if $P_1 = P_2 = P_3 = 0$ or $P_2 = P_5 = P_8 = 0$ as well as 5.14 are satisfied. Now if we set that $x^2 + y^2 + z^2 = 1$ since it has to be on the unit sphere, the inverse calculation from the coefficients $\mathbf{P}$ to the parameters could be obtained by:

$$\begin{aligned}
&x = \frac{P_1}{\sqrt{P_1^2+P_2^2+P_3^2}},\ y = \frac{P_2}{\sqrt{P_1^2+P_2^2+P_3^2}},\ z = \frac{P_3}{\sqrt{P_1^2+P_2^2+P_3^2}} \\
&or \\
&x = \frac{P_4}{\sqrt{P_4^2+P_5^2+P_6^2}},\ y = \frac{P_5}{\sqrt{P_4^2+P_5^2+P_6^2}},\ z = \frac{P_6}{\sqrt{P_4^2+P_5^2+P_6^2}} \\
&or \\
&x = \frac{P_7}{\sqrt{P_7^2+P_8^2+P_9^2}},\ y = \frac{P_8}{\sqrt{P_7^2+P_8^2+P_9^2}},\ z = \frac{P_9}{\sqrt{P_7^2+P_8^2+P_9^2}}
\end{aligned} \tag{5.15}$$

$$\begin{aligned}
&a : b : c : d = P_1 : P_4 : P_7 : xP_{10} \\
&or \\
&a : b : c : d = P_2 : P_5 : P_8 : yP_{10} \\
&or \\
&a : b : c : d = P_3 : P_6 : P_9 : zP_{10}
\end{aligned}$$

Thus, spherical circular constraint can now be represented in terms of

geometric constraints given by Eq. 5.9. By setting $q_4 = 1$ we can project the quadric into three-dimensional image space. It can be shown that the manifold is a hyperboloid with one sheet[12]. Figure. 5.2 shows one example of the manifold in 3D image space for an RR spherical dyad.

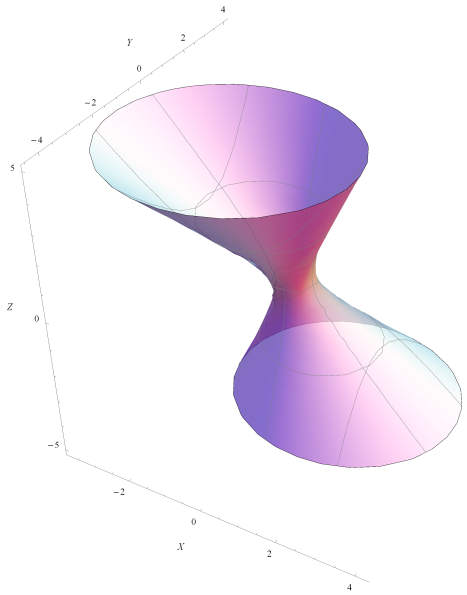

Figure 5.2: The image space manifold of the quadric in 5.9 for the spherical circular constraint is defined as follows: its center on the sphere is $C = (0.4243, 0.5657, -0.7071)$ and its radius that represented by the sphere center angle is $\alpha = 64.9°$.

5.4 Algebraic Fitting Method for Synthesizing Spherical Circular Constraints

In the previous section, we have formulated a spherical circular constraint (usually realized by a spherical RR dyad) in forms of an image space quadratic

manifold, based on which in this paper we propose an approach that could be separated into two steps: first is finding a pencil of quadrics that could best fit the given positions in least square sense, and second is identifying the quadric with coefficients that are qualified to associated with the parameters of a spherical circular constraint from the pencil of quadrics.

5.4.1 Least Square Fitting of a Pencil of Quadrics

Now consider the problem of fitting a pencil of quadrics to a set of N image points. This problem can be formulated as an over-constrained linear problem $[A]\mathbf{P} = 0$ obtained by substituting for the given values of the image points using Eq. 5.9, where $\mathbf{P}$ is the column vector of homogeneous coefficients $P_i (i = 1 \ldots 10)$. The coefficient matrix $[A]$ is given by:

$$[A] = \begin{bmatrix} A_{1_1} & A_{1_2} & A_{1_3} & A_{1_4} & A_{1_5} & A_{1_6} & A_{1_7} & A_{1_8} & A_{1_9} & A_{1_{10}} \\ \vdots & & & & & & & & & \vdots \\ \vdots & & & & \ddots & & & & & \vdots \\ \vdots & & & & & & & & & \vdots \\ A_{N_1} & A_{N_2} & A_{N_3} & A_{N_4} & A_{N_5} & A_{N_6} & A_{N_7} & A_{N_8} & A_{N_9} & A_{N_{10}} \end{bmatrix} \tag{5.16}$$

where, for the ith image points, we have

$$\begin{aligned} A_{i_1} &= q_{i4}^2 + q_{i1}^2 - q_{i2}^2 - q_{i3}^2, \quad A_{i_2} = 2(q_{i_1} q_{i_2} - q_{i_4} q_{i_3}), \\ A_{i_3} &= 2(q_{i_1} q_{i_3} + q_{i_4} q_{i_2}), \quad A_{i_4} = 2(q_{i_1} q_{i_2} + q_{i_4} q_{i_3}), \end{aligned} \tag{5.17}$$

$$
\begin{aligned}
A_{i_5} &= q_{i_4}^2 - q_{i_1}^2 + q_{i_2}^2 - q_{i_3}^2, \quad A_{i_6} = 2(q_{i_2}q_{i_3} - q_{i_4}q_{i_1}), \\
A_{i_7} &= 2(q_{i_1}q_{i_3} - q_{i_4}q_{i_2}), \quad A_{i_8} = 2(q_{i_2}q_{i_3} + q_{i_4}q_{i_1}), \\
A_{i_9} &= q_{i_4}^2 - q_{i_1}^2 - q_{i_2}^2 + q_{i_3}^2, \quad A_{i_{10}} = q_{i_1}^2 + q_{i_2}^2 + q_{i_3}^2 + q_{i_4}^2.
\end{aligned}
$$

In linear algebra, the Singular Value Decomposition (SVD) [84] of an $N \times 10$ matrix $[A]$ is a factorization of the form:

$$
[A] = [U][S][V]^T \tag{5.18}
$$

where $[U]$ is an $N \times N$ orthonormal matrix, whose N columns, called the *left singular vectors* of $[A]$, are the eigenvectors of $[A][A]^T$; $[S]$ is an $N \times 10$ rectangular diagonal matrix with 10 non-negative real numbers on the diagonal, whose values σ_1 through σ_{10} are square roots of the eigenvalues of $[A][A]^T$ (or equivalently $[A]^T[A]$); and $[V]^T$ is an 10×10 orthonormal matrix, whose 10 columns, called the *right singular vectors*, are the eigenvectors of $[A]^T[A]$.

The over-constrained system of linear equations, $[A]\mathbf{P} = 0$, can be solved as a total least squares minimization problem with the constraint $\mathbf{P}^T\mathbf{P} = 1$. Also, it is obvious that those orthonormal singular vectors that associated with the least singular values are the least square solutions to $[A]\mathbf{P} = 0$.

In views of 5.9, the least square solutions of $[A]\mathbf{P} = 0$ might not be necessarily qualified to represent a spherical circular constraint because they may not satisfy the four conditions Eq. 5.13. Therefore, the next step is to identify those "appropriate" solutions from all the linear combinations of the singular

vectors of the least singular values:

$$\mathbf{P} = \alpha_1\mathbf{v}_1 + \alpha_2\mathbf{v}_2 + \alpha_3\mathbf{v}_3 + \alpha_4\mathbf{v}_4 + \alpha_5\mathbf{v}_5. \tag{5.19}$$

Here we take five singular vectors $\mathbf{v_1}$ through $\mathbf{v_5}$ since there are four equations in 5.13 to be satisfied and the fact that they are all homogeneous. Substituting 5.19 into 5.13 we obtain 4 homogeneous quadratic equations. Since α_1 through α_5 are also homogeneous, for simplification purpose, α_1 can be set to be 1 such that these 4 homogeneous equations become non-homogenous. A lot of numerical algorithms could handle a group of these quadratic equations. One example is the `NSolve` command in `Mathematica` software, which can solve our 4 equations instantly.

To measure the error e_c of a vector $\mathbf{P}$ in qualifying to be associated with an spherical circular constraint, we have:

$$\begin{aligned} E &= [P_1P_5 - P_2P_4]^2 + [P_1P_6 - P_3P_4]^2 + [P_2P_6 - P_3P_5]^2 \\ &+[P_4P_8 - P_5P_7]^2 + [P_4P_9 - P_6P_7]^2 + [P_5P_9 - P_6P_8]^2 \\ &+[P_1P_8 - P_2P_7]^2 + [P_1P_9 - P_3P_7]^2 + [P_2P_9 - P_3P_8]^2 \\ e_c &= \sqrt{E}. \end{aligned} \tag{5.20}$$

where P_i are given by 5.19.

Furthermore, we also need to measure the surface fitting error e_s for the image points of the prescribed positions, i.e., the error function that tells us if the constraint manifold we find with our approach fits the given image points

well. Considering in 5.18 the singular values σ in $[S]$ actually reflect the least-square error of the algebraic fitting for the given data $[A]$ to the manifold parameter $\mathbf{P}$, based on the expression of the resulting parameter vector $\mathbf{P}$ in 5.19 we can write the surface fitting error function as:

$$e_s = \sqrt{\frac{\alpha_1^2\sigma_1^2+\alpha_2^2\sigma_2^2+\alpha_3^2\sigma_3^2+\alpha_4^2\sigma_4^2+\alpha_5^2\sigma_5^2}{\alpha_1^2+\alpha_2^2+\alpha_3^2+\alpha_4^2+\alpha_5^2}}. \tag{5.21}$$

and e_s will be utilized as the surface fitting measurement.

5.5 Synthesis of 4R Linkages using Software

A web based graphical tool has been developed using *Mathematica* to implement the algorithm mentioned above.The process of designing the mechanism using the software and the algorithm used is explained below using an example.Here, we consider an exact spherical four-bar $RRRR$ coupler motion for illustration purpose. The linkage parameters for $RRRR$ example are as follows: the two fixed pivots P_1 and P_2 are located at $(-1, 0, 0)$ and $(0, 1, 0)$ on the sphere, respectively, and the sphere center angle of the link lengths of the crank link, coupler link and output link are 30°, 60° and 75°, respectively. We sample 12 positions from this motion as given in Table 5.1. These 12 positions are also plotted in Figure. 5.3.These positions serve as in input for the software.

Table 5.1: The rotation of the 12 given spherical positions represented in quaternion format.

Position	q_1	q_2	q_3	q_4
1	0.2456	0.4356	0.7485	0.4356
2	0.1852	0.3981	0.7591	0.4806
3	0.1349	0.3584	0.7501	0.5391
4	0.1027	0.3194	0.7237	0.6030
5	0.0907	0.2857	0.6828	0.6663
6	0.0968	0.2625	0.6299	0.7245
7	0.1167	0.2550	0.5669	0.7746
8	0.1450	0.2677	0.4957	0.8134
9	0.1759	0.3038	0.4195	0.8371
10	0.2038	0.3623	0.3446	0.8417
11	0.2261	0.4348	0.2821	0.8247
12	0.2456	0.5060	0.2456	0.7895

Table 5.2: Singular values of $[A]$

2.51×10^{-16}	2.38×10^{-15}	0.0007	0.0080	0.0173	0.0872	0.2786	1.0317	2.1011	6.5142

5.5.1 Design Process

Now we start from these given position data in Table 5.1 to test if our approach can successfully identify the two circular constraints. The size for matrix $[A]$ as in Eq. 5.16 is 12×10. The first step is to find the singular values and their corresponding singular vectors of $[A]$ via Singular Value Decomposition. The singular values are listed in Table 5.2 in the increasing order of magnitude. Note that there are two singular values that are almost zero. This is because

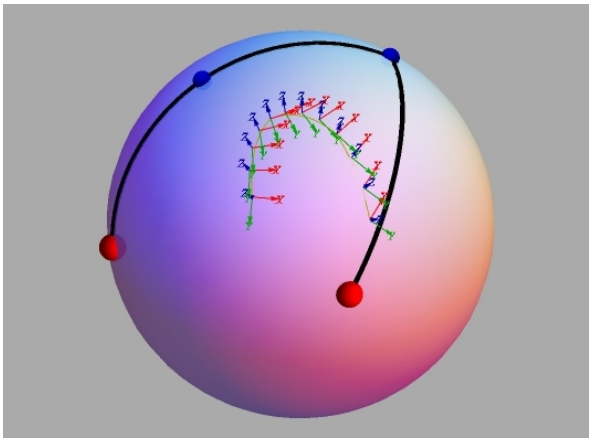

Figure 5.3: 12 given positions on the sphere as displayed by the software.

our data is perfectly curve data, i.e., they lie exactly on the intersection of two hyperboloids. Next, we take five smallest eigenvalues and their associated singular vectors ($\mathbf{v}_1$ through $\mathbf{v}_5$) are listed in Table 5.3. From the constraint fitting error e_c in the table we can tell that none of these five manifolds is qualified to define a valid spherical circular constraint even though the 12 given positions fit them quite well.

By constructing 5.19 and substituting it into 5.13, we obtain 4 homogeneous quadratic equations. Letting α_1 equals to 1 makes them non-homogeneous and hereby able to be solved with very simple numerical algorithms. Among the roots of these 4 equations, complex ones are excluded, as well as those roots that will lead to $P_1 = P_2 = P_3 = 0$ or $P_2 = P_5 = P_8 = 0$ but cannot

Table 5.3: Five orthonormal singular vectors that correspond to five smallest singular values as in Table. 5.2. The last column e_c indicates the error of constraint fitting, which is defined by 5.20. Any value smaller than 10^{-4} in the vector is shown as zero to save space.

P_1	P_2	P_3	P_4	P_5	P_6	P_7	P_8	P_9	P_{10}	e_c
0	-0.35	0.61	0	0.11	0.19	0	0	0	-0.67	0.13
0	-0.14	0.25	0	-0.47	-0.82	0	0	0	-0.01	0.24
-0.15	0.43	-0.20	0.54	0.07	-0.17	-0.12	0.17	0.39	-0.45	0.43
-0.32	0.27	0.33	-0.22	0.16	-0.04	0.23	-0.53	0.50	0.17	0.45
-0.52	-0.32	-0.21	-0.18	0.55	-0.32	0.18	0.29	-0.07	-0.03	0.49

Table 5.4: Four groups of valid solutions for α_1 through α_5. e_c and e_s indicates their constraint fitting error and surface fitting error in Eq. 5.20 and Eq. 5.21, respectively.

Sol^n	α_1	α_2	α_3	α_4	α_5	e_c	e_s
1	1	0.2378	-9.08×10^{-9}	-3.06×10^{-11}	-1.24×10^{-12}	4.63×10^{-9}	2.50×10^{-16}
2	1	-2.3769	-1.01×10^{-8}	5.66×10^{-10}	-1.26×10^{-10}	1.29×10^{-8}	2.40×10^{-16}
3	1	10.4409	6.4721	-0.3098	-0.3305	1.87×10^{-9}	0.0006
4	1	0.0782	0.0162	-0.6113	-0.3588	1.10×10^{-9}	0.0064

make Eq. 5.14 satisfied. The rest valid solutions and their constraint fitting error e_c as well as surface fitting error e_s are listed in Table. 5.4.

In the column of e_c, since the 4 quadratic equations are constructed based on the constraint fitting, all the solutions fit the constraint perfectly. Also, from the surface fitting error e_s we can see that the constraint manifold defined by the first two groups of solutions fit the given data perfectly, while the last two groups of solutions contains some error in given data fitting. Therefore,

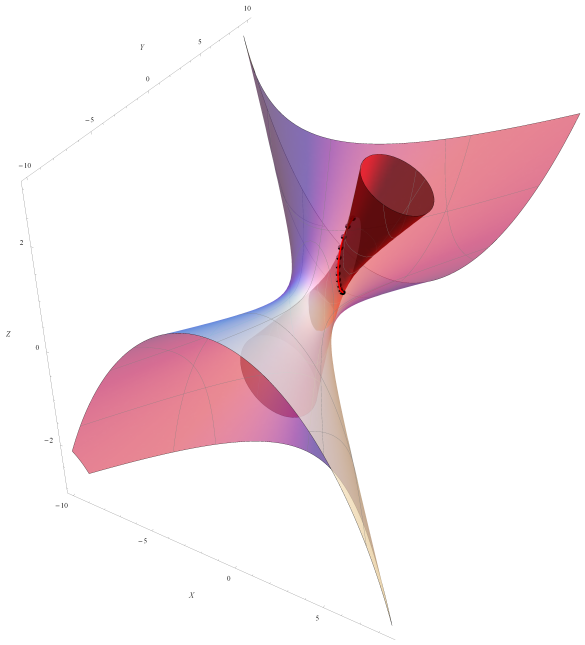

Figure 5.4: Two resulting constraint manifolds identified from a pencil of quadrics; the manifolds are hyperboloids of one sheet that satisfy the conditions imposed by Eq. 5.13; the 12 black image points lying on the intersection curve in the figure denote 12 given positions in Table 5.1.

we choose the first two groups as our final choice, and find the two resulting coefficient vectors by 5.19. These two constraint manifolds are plotted in Fig. 5.4; the 12 image points in the figure denote 12 given positions in Table 5.1 and lie on the intersection of the two manifolds.

By observing the first two groups of solutions, we can find that the final resulting coefficient vector $\mathbf{P}$ defined by 5.19 is only consisted with the first

Table 5.5: The dimensions of the two resulting spherical RR dyads:

vector	$a : b : c : d$	x	y	z
$\mathbf{v}_{r1}$	$1 : 0.0000 : 0.0000 : 0.8660$	0.0000	0.5000	-0.8660
$\mathbf{v}_{r2}$	$0.0000 : 1 : 0.0000 : -0.2588$	0.0000	-0.5000	-0.8660

two singular vectors, whose associated singular values are zero as shown in Table. 5.2. This is because our given data is perfect, and our expected results are supposed to lie within the exact null space of $[A]$, which for perfect given data is the singular-plane defined by the two singular vectors of zero singular values.So the software selects the two dyads based on the least constraint error e_c.

Furthermore, by applying the inverse computation given by Eq. 5.15 on the two resulting coefficient vectors,the dimensions of the parameters of the two resulting circular constraints are also listed in Table. 5.5 as obtained by the software and it is easily verified that the two dyads combined together constrain the motion of the spherical $RRRR$ linkage as given.

5.6 Conclusion

This work is extension of previous work [1] on planar four-bar synthesis case to spherical four-bar linkage synthesis. There are simply by two steps in the approach. Since we have formulated the data fitting process in linear form($[A]\mathbf{P} = 0$), the first step is finding a pencil of general quadratic mani-

folds in the image space that best fit the given image points in the least squares sense, which is done by using Singular Value Decomposition and solving for the singular vectors. The singular vectors associated with the smallest singular values are then linearly combined to define the coefficients of a pencil of quadrics. Second, four additional constraints on the linear coefficients are then imposed to identify the quadric that qualified to represent a spherical circular constraint from the pencil of quadrics. After the inverse computation converting the quadric coefficients to the spherical four bar parameters, a spherical four bar linkage that best guides through the set of given displacements can be obtained. The resulting algorithm for spherical four-bar linkage synthesis is vastly more efficient.

Bibliography

[1] Ge, Q. J., Zhao, P., Li, X., Purwar, A., 2012, "A Novel Approach to Algebraic Fitting of Constraint Manifolds For Planar 4R Motion Approximation", ASME 2012 International Design Engineering Technical Conferences and Computers and Information in Engineering Conference, Chicago, Paper No. DETC2012-71190

[2] Purwar, A., Jin, Z, Ge, Q.J., 2008, "Computer Aided Synthesis of Piecewise Rational Motions for Spherical 2R and 3R Robot Arms", *Journal of Mechanical Design*, Vol. 130 / 112301-1.

[3] Hayes, M. J. D., and Rusu, S. R., 2011. "Quadric surface fitting applications to approximate dimensional synthesis.". In 13th World Congress in Mechanism and Machine Science,19-23 June, 2011.

[4] Purwar, A., Jin, Z, Ge, Q.J., 2008, "Rational Motion Interpolation Under Kinematic Constraints of Spherical 6R Closed Chains", *Journal of Mechanical Design*, Vol. 130 / 062301-1

[5] Merlet, J. P., 2006. Parallel Robots. Springer.

[6] Blaschke, W., 1911. "Euklidische kinematik und nichteuklidische geometrie". *Zeitschr. Math. Phys.,* **60**, pp. 61–91 and 203–204.

[7] Ge, Q.J., and Larchelle, P., 1999, "Algebraic Motion Approximation With NURBS Motions and Its Application to Spherical Mechanism Synthesis", J. Mech. Des.,121(4): 529-532.

[8] Grunwald, J., 1911. "Ein abbildungsprinzip, welches die ebene geometrie und kinematik mit der raumlichen geometrie verknupft". *Sitzber. Ak. Wiss. Wien,* **120**, pp. 677–741.

[9] Ravani, B., and Roth, B., 1983. "Motion synthesis using kinematic mappings". *Journal of Mechanisms Transmissions and Automation in Design-Transactions of the Asme,* **105**(3), pp. 460–467.

[10] Ravani, B., and Roth, B., 1984. "Mappings of spatial kinematics". *Journal of Mechanisms Transmissions and Automation in Design-Transactions of the ASME,* **106**(3), pp. 341–347.

[11] Bottema, O., and Roth, B., 1979. *Theoretical Kinematics.* North Holland, Amsterdam.

[12] McCarthy, J. M., 1990. *Introduction to Theoretical Kinematics.* MIT, Cambridge, Mass.

[13] Ge, Q. J., and Ravani, B., 1994. "Computer-aided geometric design of motion interpolants". *ASME Journal of Mechanical Design,* **116**(3), pp. 756–762.

[14] Ge, Q. J., and Ravani, B., 1994. "Geometric construction of bezier motions". *ASME Journal of Mechanical Design,* **116**(3), pp. 749–755.

[15] Juttler, B., and Wagner, M. G., 1996. "Computer-aided design with spatial rational b-spline motions". *ASME Journal of Mechanical Design,* **118**(2), pp. 193–201.

[16] Wagner, M. G., 1994. "A geometric approach to motion design". Ph.d. dissertation.

[17] Chiang, C. H.,2000 "Kinematics of spherical mechanisms." *Krieger Pub* Malabar, FL.

[18] Kraal, J. C. and Vance, J. M.,2001 "VEMECS: a virtual reality interface for spherical mechanism design." *Journal of Engineering Design,,***12**,(3),pp. 245–254.

[19] Purwar, A., Anantwar, S., Zhao, P., 2012, "An Interactive Approach to Designing Planar Parallel Manipulators using Image Space Representation," ASME 2012 International Design Engineering Technical Conferences and Computers and Information in Engineering Conference, Chicago, Paper No. DETC2012-70880

[20] Furlong, T. and Vance, J. and Larochelle, P.,1999 "Spherical Mechanism Synthesis in Virtual Reality". *ASME Journal of Mechanical Design,***121**(4), pp. 515–520.

[21] Ketchel, J. S. and Larochelle, P. M.,2007 "Computer-aided manufacturing of spherical mechanisms." *Mechanism and Machine Theory,***42**,pp. 131–146.

[22] Röschel, O., 1998. "Rational motion design - a survey". *Computer-Aided Design,* **30**(3), pp. 169–178.

[23] Purwar, A., Chi, X., and Ge, Q. J., 2008. "Automatic fairing of two-parameter rational b-spline motion". *ASME Journal of Mechanical Design,* **130**(1), p. 011003.

[24] Purwar, A., and Ge, Q. J., 2005. "On the effect of dual weights in computer aided design of rational motions". *ASME Journal of Mechanical Design,* **127**(5), pp. 967–972.

[25] Bodduluri, R. M. C., and McCarthy, J. M., 1992. "Finite position synthesis using image curve of a spherical four-bar motion". *ASME J. of Mechanical Design,* **114**(1).

[26] D.A.Ruth, J.M.McCarthy 1999, "The design of spherical 4R linkages for four specified orientations", *Mechanism and Maching Theory*, 34(5):677-692.

[27] Bodduluri, R., 1990. "Design and planned movement of multi-degree of freedom spatial mechanisms". Ph.d. dissertation.

[28] Larochelle, P., 1994. "Design of cooperating robots and spatial mechanisms". Phd dissertation.

[29] Hayes, M. J. D., Luu, T., and Chang, X.-W., 2004. *Kinematic Mapping Application to Approximate Type and Dimension Synthesis of Planar Mechanisms*. 9th Advances in Robotic Kinematics. Kluwer Academic Publishers, Dordrecht, The Netherlands.

[30] Brunnthaler, K., Schrocker, H., and Husty, M., 2006. *Synthesis of spherical four-bar mechanisms using spherical kinematic mapping*. Advances in Robot Kinematics. Springer, Netherlands.

[31] Venkataramanujam, V., and Larochelle, P., 2007. "Approximate motion synthesis of spherical kinematic chains". In Proceedings of ASME 2007 International Design Engineering Technical Conferences & Computers and Information in Engineering, Paper No. DETC2007-34372.

[32] Hayes, M. J. D., and Husty, M., 2003. "On the kinematic constraint surfaces of general three-legged planar robot platforms". Mechanism and Machine Theory, **38**(379394).

[33] Hayes, M., 1999. "Kinematics of general planar stewart-gough platforms". Ph.d. dissertation.

[34] Brunnthaler, K. and Schrocker, H.-P. and Husty, M., 2006, "Synthesis of spherical four-bar mechanisms using spherical kinematic mapping", *Advances in Robot Kinematics*, pp. 377–385.

[35] Hayes, M. J. D., Zsombor-Murray, P. J., and Chen, C., 2004. "Kinematic analysis of general planar parallel manipulators". ASME J. of Mechanical Design, **126**(5).

[36] Murray, A. P., Pierrot, F., Dauchez, P., and McCarthy, J. M., 1997. "A planar quaternion approach to the kinematic synthesis of a parallel manipulator". Robotica, **15**, pp. 361-365. Article Part 4.

[37] Wu, J., Purwar, A., and Ge, Q. J., 2010, "Interactive Dimensional Synthesis and Motion Design of Planar 6R Single-Loop Closed Chains via Constraint Manifold Modification". *ASME Journal of Mechanisms and Robotics,* **2**, pp. 31012(8 pages)

[38] Purwar, A., Wu, J., Gupta, A., Ge, Q.J., 2010, "A Visual, Interactive Approach to Synthesis of Spherical 6R Closed Chains for Rational Motions via Constraint Manifold Modification". In 2010 ASME Mechanisms and Robotics Conference, Montreal, Canada, August 15-18, Paper No. DETC2010-28874.

[39] RUBEL, A. J., and KAUFMAN, R. E., 1977. "Kinsyn III: A new human-engineered system for interactive computer-aided design of planar linkages". *ASME Journal of Engineering for Industry,* **99**, p. 440448.

[40] Erdman, A., and Gustafson, J., 1977. Lincages: Linkage interactive computer analysis and graphically enhanced synthesis packages,. Tech. rep.

[41] Erdman, A. G., and Riley, D., 1981. "Computer-aided linkage design using the lincages package". In ASME Design Engineering Technical Conferences, ASME Press. Paper Number 81-DET-121.

[42] Kihonge, J., Vance, J., and Larochelle, P., 2001. "Spatial mechanism design in virtual reality with networking". In ASME 2001 Design Engineering Technical Conferences.

[43] Larochelle, P. M., 1998. "Spades: Software for synthesizing spatial 4C linkages". In ASME Design Engineering Technical Conferences (DETC).

[44] Larochelle, P. M., Dooley, A. P., Murray, A. P., and McCarthy, J. M., 1993. "Sphinx: Software for synthesizing spherical 4R mechanisms". In NSF Design and Manufacturing Systems Conference, pp. 607-611.

[45] Ruth, D., and McCarthy, J. M., 1997. "Sphinxpc: An implementation of four position synthesis for planar and spherical 4R linkages". In ASME Design Engineering Technical Conferences (DETC).

[46] Tse, D., and Larochelle, P. M., 1999. "Osiris: a new generation spherical and spatial mechanism cad program". In 1999 Florida Conference on Recent Advancements in Robotics.

[47] Perez, A., and McCarthy, J., 2000. "Dimensional synthesis of spatial RR robots". In Advances in Robot Kinematics.

[48] Su, H., and McCarthy, J. M., 2001. "Classification of designs for RRSS linkages". In ASME Design Engineering Technical Conferences.

[49] Su, H., Collins, C., and McCarthy, J. M., 2002. "An extensible java applet for spatial linkage synthesis". In 2002 ASME Design Engineering Technical Conferences, ASME.

[50] SyMech. http://www.symech.com/.

[51] WATT. http://www.heron-technologies.com.

[52] Sandor, G. N., and Erdman, A. G., 1997. *Advanced Mechanism Design: Analysis and Synthesis Vol. 2*. Prentice-Hall, Englewood Cliffs, NJ.

[53] Suh, C. H., and Radcliffe, C. W., 1978. *Kinematics and Mechanism Design*. Wiley, New York.

[54] McCarthy, J. M., 2000. *Geometric Design of Linkages*. Springer-Verlag, New York.

[55] Farin, G., 1996. *Curves And Surfaces for Computer-Aided Geometric Design: A Practical Guide*, 4th ed. Academic Press, New York.

[56] Hoschek, J., and Lasser, D., 1993. *Fundamentals of Computer Aided Geometric Design*. A K Peters.

[57] Piegl, L., and Tiller, W., 1995. *The NURBS Book*. Springer, Berlin.

[58] Nintendo Wii Motion Control Gaming Platform, http://www.nintendo.com/wii

[59] Microsoft Kinect Motion Control Platform, http://www.xbox.com/en-US/kinect

[60] Eberly, D., 2002. Rotation representations and performance issue. Technical report, Magic Software, Inc.

[61] Rakotomanga, N., Chablat, D., Caro, S., 2008. "Kinetostatic performance of a planar parallel mechanism with variable actuation," In the proceedings of 11th International Symposium on Advances in Robot Kinematics, Kluwer Academic Publishers, Nantes, France.

[62] Arakelian, V., Briot, S., Glazunov, V., 2008. "Increase of singularity-free zones in the workspace of parallel manipulators using mechanisms of variable structure," Mechanism and Machine Theory, **43**(9), pp. 1129–1140

[63] Chablat, D., Wenger, P., 1998. "Working Modes and Aspects in Fully-Parallel Manipulator," In Proceeding IEEE International Conference on Robotics and Automation, pp. 1964–1969.

[64] Wenger, 2004. "Uniqueness domains and regions of feasible paths for cuspidal manipulators," IEEE Transactions on Robotics, **20**(4), pp. 745–750.

[65] Jin, Z., and Ge, Q. J., 2007. "Rational motion interpolation under kinematic constraints of planar 6R closed chain" In ASME 2007 International Design Engineering Technical Conferences & Computers and Information in Engineering Conference, ASME Press. Paper No. DETC2006–99650.

[66] Purwar, A., Jin, Z., and Ge, Q. J., 2008. "Rational motion interpolation under kinematic constraints of spherical 6r closed chains", ASME Journal of Mechanical Design, **130**(6), pp. 0623011 - 0623019.

[67] Purwar, A., Gupta, A., 2011. "Visual Synthesis of RRR- and RPR-Legged Planar Parallel Manipulators using Constraint Manifold Geometry", In ASME 2011 International Design Engineering Technical Conferences & Computers and Information in Engineering Conference, ASME Press. Paper No. DETC2011–48830.

[68] Ge, Q., J., 1990. "Kinematic constraints as algebraic manifolds in the clifford algebra of projective three space", Ph.d. dissertation.

[69] Jin, Z., 2007. "Computer aided synthesis of rational motions under kinematic constraints", Ph.d. dissertation.

[70] Bonev, I., Zlatanov, D., Gosselin, C., 2003. "Singularity Analysis of 3-DOF Planar Parallel Mechanisms via Screw Theory", ASME Journal of Mechanical Design, **125**(9), pp. 573 - 581.

[71] Perez, A., and McCarthy, J., M., 2004. "Dual quaternion synthesis of constraint robotic systems", ASME Journal of Mechanical Design, **126**(3), pp. 425 - 435.

[72] Larochelle, P., and McCarthy, J., M., 1994. "Design of spatial 4c mechanisms for rigid body guidance". In Proc. 1994 ASME Mechanisms Conference, pp. 135 - 142.

[73] Zhao, P., spring 2011. “Formulation of Kinematic Constraints Manifolds in Quaternion Space for Planar Parallel Manipulator”. MEC572 project, Stony Brook University (advised by Prof A. Purwar).

[74] Tsai, L., W., Robot Analysis, the Mechanics of Serial and Parallel Manipulators, John Wiley & Sons, New York, USA, 1999.

[75] Zhang, B., and Crane, C., Special Singularity Analysis for a 6-DOF Parallel Platform”. 10th Int. Conference on Robotics & Remote Systems for Hazardous Environments, Gainesville, FL, USA, 2004.

[76] Mohammadi, Daniali, H., R.,Zsombor-Murray,J., P., and Angeles, J., 1995.”Singularity Analysis of Planar Parallel Manipulators”.Mech. Math. Theory Vol. 30, No. 5, pp. 665-678.

[77] O. Ma and J. Angeles, Int. J. Robotics Automatn 7(1), 23-29 (1992).

[78] Gough, V., E., and Whitehall, S., G., ”Universal Tyre Test Machine,” Proceedings of the FISITA Ninth Int. Technical Congress, London, UK, pp. 117-137, 1962.

[79] Stewart, D., ”A Platform with Six Degrees of Freedom,” Proc of the IMechE, Vol. 180, Pt. 1, No. 15, pp. 371 - 385, 1965-66.

[80] Arsenault, M., and Boudreau, R., 2004. ”The synthesis of Three-Degree-of-Freedom Planar Parallel Mechanisms with Revolute Joints (3-RRR) for an Optimal singulariy-Free Workspace”. Journal of Robotic Systems 21(5), pp. 259 274 .

[81] Carretero, J., A., Podhorodeski, R., P., Nahon, M., A., and Gosselin, C., M., 2000. "Kinematic Analysis of a New Three Degree-of-Freedom spatial Parallel Manipulator", ASME Journal of Mechanical Design, **122**(3), pp. 17 - 24.

[82] Ceccarelli, M., Carbone, G., Ottaviano, E. "An Optimization Problem Approach for Designing both Serial and Parallel Manipulators". Proceedings of MUSME 2005, the International Symposium on Multibody Systems and Mechatronics Uberlandia (Brazil), 6-9 March 2005 Paper no. XX-MUSME05

[83] Williams II, R., Shelley, B., 1997. "Inverse Kinematics for Planar Parallel Manipulators", In ASME 1997 International Design Engineering Technical Conferences, ASME Press. Paper No. DETC97/DAC–3851.

[84] Golub, G. and Van Loan, C., 1996. "Matrix Computations", Johns Hopkins Univ Press, Baltimore, MD

[85] Sommerville, D.M.Y., 1959. "Analytical geometry of three dimensions", Cambridge University Press.

[86] Kim, H., Tsai, L., 2003. "Design Optimization of a Cartesian Parallel Manipulator". *ASME Journal of Mechanical Design,* **125**(3), pp. 43 - 51.

[87] Kim, H., Tsai, L., 2003. "Kinematic Synthesis of a Spatial 3-RPS Parallel Manipulator". *ASME Journal of Mechanical Design,* **125**(3), pp. 92 - 97.

[88] Affi, Z., Romdhane, L., and Maalej, A., 2004. "Dimensional Synthesis of a 3-Translational-DOF in-Parallel Manipulator for a Desired Workspace". *European Journal of Mechanics A/Solids,* **23**, pp. 311 - 324.

[89] Rao, N., Rao, K., 2009. "Dimensional Synthesis of a Spatial 3-RPS Parallel Manipulator for a Prescribed Range of Motion of Spherical Joints". *Journal of Mechanism and Machine Theory,* **44**, pp. 477 - 486.

[90] Rao, N., Rao, K., 2009. "Dimensional Synthesis of a Spatial 3-RPS Parallel Manipulator for a Prescribed Range of Motion of Spherical Joints". *Journal of Mechanism and Machine Theory,* **44**, pp. 477 - 486.

[91] Mruthyunjaya, T. S., 2003. "Kinematic structure of mechanisms revisited". *Journal of Mechanism and Machine Theory,* **38**(4), pp. 279 - 320.

[92] Angeles, J., 2004. "The Quantitative Synthesis of Parallel Manipulators". *ASME Journal of Mechanical Design,* **126**(7), pp. 617 - 624.

[93] Bai, s., 2010. "Optimum design of spherical parallel manipulators for a prescribed workspace". *Journal of Mechanism and Machine Theory,* **45**, pp. 200 - 211.

[94] Li, Y., Xu, Q., 2006. "Kinematic Analysis and Design of a New 3-DOF Translational Parallel Manipulator". *ASME Journal of Mechanical Design,* **128**(7), pp. 729 - 737.

[95] Jin, Y., Chen, I., and Yang, G., 2009. "Kinematic design of a Family of 6-DOF Partially Decoupled Parallel Manipulators". *Journal of Mechanism and Machine Theory,* **44**, pp. 912 - 922.

[96] Liu, X., Guan, L., and Wang, J., 2007. "Kinematics and Closed Optimal Design of a Kind of PRRRP Parallel Manipulator". *ASME Journal of Mechanical Design,* **129**(5), pp. 558 - 563.

[97] Altuzarra, O., Pinto, C., Sandru, B., Hernandez, A., 2011. "Optimal Dimensioning for Parallel Manipulators: Workspace, Dexterity, and Energy". *ASME Journal of Mechanical Design,* **133**(4), p. 041007-1.